TUM

Technische Universität München

Department of Mathematics

Master's Thesis

Robust numerical discretizations
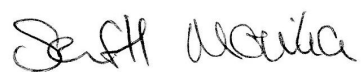# for dynamic phase-field fracture

Monika Senftl

Supervisor: Prof. Dr. Boris Vexler

Advisor: Prof. Dr. Thomas Wick

Submission Date: December 15, 2017

I assure the single handed composition of this master's thesis only supported by declared resources.

Garching, December 15, 2017

Zusammenfassung

Die Prognose von Rissentstehung und -ausbreitung in Feststoffen, durch computergestützte Modelle, ist ein großes aktuelles Forschungsthema in der Maschinen-, Energie- und Umwelttechnik. Ziel dieser Thesis ist der Vergleich von quasi-statischen und dynamischen Phasenfeld-Rissmodellen mit unterschiedlichen Zeitschrittverfahren, basierend auf Genauigkeit und Rechenkosten.

Hierfür wird die Phasenfeld-Struktur eines Probekörpers mit sprödem Material untersucht. Man kann das quasi-statische Phasenfeld-Problem in ein System gekoppelter partieller Differentialgleichungen überführen, um so durch zeitliche und räumliche Diskretisierung an dessen numerische Lösung zu gelangen. Für die zeitliche Komponente wird das Verfahren von Galerkin, eine Finite Elemente Methode, benutzt. Für den räumlichen Part erstellen wir einen sogenannten *adaptive error-oriented Newton algorithm*, der als innere Schleife in einer *inexact augmented Lagragian iteration* läuft. Anschließend wird das Modell mit Zeitableitungen auf den dynamischen Fall erweitert und ebenfalls analysiert. Mit Hilfe von Einschrittverfahren, den sogenannten One-Step-θ-Schemes, können unterschiedliche Zeitschrittverfahren, wie expliziter und impliziter Euler, oder auch Crank-Nicolson, einfach dargestellt und numerisch berechnet werden.

In einem numerischen Beispiel, dem *Single edged notched shear test*, wird das quasi-statische, als auch das dynamische System zusammen mit verschiedenen Zeitschrittverfahren verglichen. Dazu wird die kostenlose, frei zugängliche Software-Bibliothek deal.II [6], mit der partielle Differentialgleichungen anhand adaptiven finiten Elementen gelöst werden können, zum Einsatz gebracht.

Nach detaillierter Analyse der Rissbilder, der Kraft-Verschiebungs-Kurven und der Newton Konvergenz kann nicht klar gesagt werden, welches System oder Zeitschrittverfahren effizienter ist. Quasi-statisches oder dynamisches Modell, impliziter Euler oder Crank-Nicolson Verfahren, alles hat seine Vor- und Nachteile.

Abstract

Fracture and therewith associated prediction of crack initiation and propagation in solids through computational models is one of the major research topics in mechanical, energy and environmental engineering these days. The goal of this thesis is a comparison of the quasi-static and the dynamic fracture model checking several time-stepping schemes, in case of accuracy and computational costs.

Therefore, the phase-field structure of a quasi-static phase-field model for mechanics in brittle materials is examined. The quasi-static phase-field problem can be converted in a partial differential equation system to get a numerical solution by studying their temporal and spatial discretizations. For the temporal component a Galerkin Finite Element scheme is used, for the spatial part an adaptive error-oriented Newton algorithm which works as an inner loop within an inexact augmented Lagrangian iteration is utilized. Subsequently, the quasi-static phase-field system is extended to the dynamic case by implementing time derivatives and will be analyzed too. With the aid of One-Step-θ schemes different time-stepping schemes, as backward Euler, implicit Euler or Crank-Nicolson, can easily be presented and numerically calculated.

In a numerical example, the *Single edged notched shear test*, a comparison of the quasi-static and the dynamic system in terms of different time-stepping schemes is given. Therefore deal.II, a free, open source C++ software library for solving partial differential equations using adaptive finite elements, is applied.

Considering the crack patterns, the load-displacement curves and the Newton convergence one can not obviously say if it is more efficient using the quasi-static or the dynamic fracture model, a backward Euler or a Crank-Nicolson time-stepping scheme. Each of them, models and time-stepping schemes, has both, advantages and drawbacks.

Contents

1 Introduction

Fracture and therewith associated prediction of crack initiation and propagation in solids through computational models is one of the major research topics in mechanical, energy and environmental engineering these days.

Theoretical foundations of the classical theory of brittle fracture in solids are given by Griffith [20] and Irwin [21], the crack propagates if the energy release rate reaches a critical values. But Griffith theory for quasi-static brittle fracture fails in predicting crack initiation since it is insufficient to determine curvilinear crack paths, crack kinking and branching angles. This bug can be overcome by variational methods based on energy minimization, as shown in Francfort and Marigo [22] and Bourdin et al. [14, 23], where Γ-convergence inspired by the work of image segmentation by Mumford an Shah [24] is used. For details on Γ-convergent approximations see, e.g., Ambrosio and Tortorelli [25]. Utilizing such a variational approach, the crack surface is approximated by an auxiliary phase-field function φ which introduces a diffusive transition zone between the broken and unbroken material. Then a solution $\{u, \varphi\}$, where u denotes the displacement field, is searched.

An alternative quasi-static formulation of phase-field approximation was given in Miehe, Hofacker and Welschinger [5, 7], where continuum mechanics and thermodynamic arguments were utilized.

The advantages of phase-field modeling for crack propagation, given in [2], are: it is a fixed-mesh approach in which remeshing is avoided. Second, crack nucleation, propagation and the path are automatically determined because the model is just based on energy minimization. There are not any additional techniques for multiple joining and branching of cracks needed. Therefore one can handle large and complex fracture networks. At least, crack propagation in heterogeneous media does not require any modification in the framework.

Later, Bourdin, Larsen and Richardson [11], Larsen, Ortner and Süli [10] and Larsen [9] described some results on a phase-field model of dynamic fracture and introduced models for sharp interface dynamic fracture. However they did not consider applications to structures of engineering interest.

Independently, there were dynamic phase-field fracture models developed which are based

on Landau-Ginzburg type phase-field evolution equations, e.g., Karma, Kessler and Levine [26]. However, we use the phase-field formulation of Bourdin-type based on Griffith's theory since it has been proven useful in engineering applications.

Borden et al. [8] extended the quasi-static model presented by Miehe et al. [5] to the dynamic case by formulating the Lagrangian for the discrete problem in terms of a displacement u and a phase-field variable φ, then applying the Euler-Lagrange equations on it, leading to the strong form equations of motion. To get a numerical solution of them, there is spatial and temporal discretization needed.

The goals of this thesis are:

- Extend the quasi-static fracture formulation to the dynamic case.

- Comparison of the quasi-static and dynamic fracture models in terms of accuracy and computational costs.

- Comparison of a backward Euler and a Crank-Nicolson scheme in fracture models.

The structure of this thesis looks as follows. First, in Chapter 2 we set the notation, symbols and spaces. In chapter 3 we determine the quasi-static partial differential equation system of phase-field fracture in strong and weak form. For temporal and spatial discretization an extrapolation is needed. For the temporal part a Galerkin Finite Element scheme is used, for the spatial part we utilize an adaptive error-oriented Newton algorithm which works as an inner loop within an inexact augmented Lagrangian iteration. Next, in Chapter 4, we extend our phase-field system to the dynamic case and get novel strong and weak forms of the equations. After a short introduction on One-Step-θ Schemes we arrive at temporal and spatial discretization. In Chapter 5 we display a numerical benchmark experiment for crack propagation, the single edged notched shear test. There we compare the quasi-static and the dynamic fracture model using different time-stepping schemes in case of accuracy and computational costs. To conclude this thesis, we summarize our results in Chapter 6.

For our numerical tests, we use deal.II[1] [6], a free, open source C++ software library for solving partial differential equations using adaptive finite elements. It is based on state-of-the-art programming techniques to provide a modern interface to the complex data structures and algorithms needed.

---

[1]see https://www.dealii.org/, accessed November 11, 2017

2 Notation, symbols and spaces

First, we introduce a few basic notations as in [1], to understand the problem of phase-field fracture, therefore we take a look at Figure 2.1. The fracture $C \subset \mathbb{R}$ is approximated with the phase-field variable φ (which will be introduced in subchapter 3.1), where the transition zone $0 < \varphi < 1$ has a thickness of ϵ on both sides of the fracture. Therefore we can define an fractured elliptic array Ω_F as:

$$\Omega_F := \{x \in \mathbb{R}^d \mid \varphi(x) < 1\}. \tag{2.1}$$

In Figure 2.2, we can see the construction of our notation. Let $B \subset \mathbb{R}^2$ ($d = 2$, we only consider the 2-dimensional case in this thesis) be the complete domain consisting of the fractured area Ω_F and the unbroken domain Ω. We apply Dirichlet and Neumann boundary conditions on ∂B which may be time-dependent non-homogeneous ones. $\partial \Omega_F$ denotes the inner boundary of the fracture range. Note that B, Ω_F and $\partial \Omega_F$ depend on the length-scale parameter ϵ which is defined as the half thickness of Ω_F.
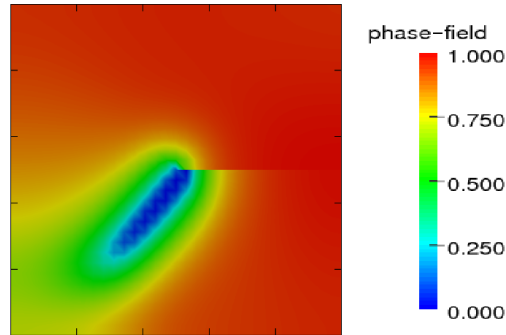

FIG. 2.1: Fracture C ($\varphi=0$) approximated with the phase-field variable φ. The transition zone $0 < \varphi < 1$ has the thickness of ϵ on both sides of the fracture.
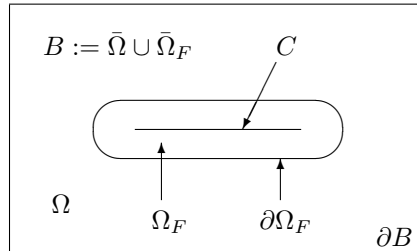

FIG. 2.2: Construction of the notation: the fracture C is approximated by the domain Ω_F including the fracture boundary $\partial \Omega_F$. Ω declares the unbroken domain. Both areas together yield the complete domain B having the outer boundary ∂B.

Next, in table 1, we give a short outline on the variables and parameters used in this thesis.

SYMBOL	DESCRIPTION	UNIT
x	position	m
t	time	s
u	displacement	m
v	velocity	m/s
∇	gradient	dimensionless
Δ	Laplace operator	dimensionless
φ	phase-field variable	dimensionless
C	crack	dimensionless
f	force	N
ϵ	positive regularization parameter	dimensionless
κ	positive regularization parameter	dimensionless
σ	Cauchy solid stress tensor	Pa/m^2
e	strain tensor	dimensionless
G_c	critical energy release rate	J/m^2
μ_s	Lamé coefficient	N/m^2
λ_s	Lamé coefficient	N/m^2
n	normal vector	dimensionless

Table 1: Variables and parameters in SI-units.

Moreover, we need a few function spaces which are introduced by:

$$V := H_0^1(B)$$
$$W_{in} := \{w \in H^1(B) \mid w \leq \varphi^{n-1} \leq 1 \ \text{ a.e. on } B\}$$
$$W := H^1(B)$$
$$L := L^2(B),$$

where $\varphi^{n-1} := \varphi(t^{n-1})$ indicates the preceded time step solution.

3 Quasi-static phase-field fracture

Based on the notations of the previous chapter, we can inspect the structure of a quasi-static phase-field model for mechanics in brittle materials. First, we introduce the associated partial differential equation system, calculate the Euler-Lagrange system of it yielding the equations which will be implemented in the numerical example of chapter 5. Next, quasi-monolithic and fully monolithic semi-linear forms are given to arrive at temporal and spatial discretization.

3.1 Equations

The partial differential equation system, we deal with in this thesis, looks as follows:

Formulation 1 *Find a vector-valued displacement u and a scalar-valued phase-field variable φ such that*

$$-\varphi \Delta u = f \quad in \ B \tag{3.1}$$

$$\varphi |\nabla u|^2 + \epsilon \Delta \varphi - \frac{1}{\epsilon}(1 - \varphi) = 0 \quad in \ B \tag{3.2}$$

$$\partial_t \varphi \leq 0 \quad in \ B, \tag{3.3}$$

with associated Dirichlet and Neumann boundary conditions

$$u = g \quad on \ \partial B_D \times I$$

$$\partial_n(\varphi u) = h \quad on \ \partial B_N \times I$$

$$\partial_n \varphi = 0 \quad on \ \partial B \times I,$$

and initial conditions

$$u(\cdot, 0) = u_0 \quad in \ B \times \{0\}$$

$$\varphi(\cdot, 0) = \varphi_0 \quad in \ B \times \{0\}.$$

System (3.1) & (3.2) is obviously quasi-static. The first equation stands for the elasticity (i.e., no crack pressure), the second one for the phase-field. The inequality constraint (3.3) presents the incompressibility. Then the associated Dirichlet and Neumann boundary conditions involving functions g and h are given, where $\partial B = \partial B_D \cup \partial B_N$ and $t \in I = [0, T]$. At least the initial conditions are shown.

The unknown solution variables are the displacement field $u : B \to \mathbb{R}^2$ and the auxiliary field variable $\varphi : B \to [0, 1]$, where $\varphi = 0$ indicates the crack region and $\varphi = 1$ denotes the unbroken material. Values between that describe a smooth transition zone depending on a positive regularization parameter ϵ.

Remark that there always holds

$$\varphi^n \leq \varphi^{n-1}, \tag{3.4}$$

because of the crack irreversibility condition (3.3). The crack can propagate in the material but is unable to heal. Due to this fact, the resulting variational inequality system is always quasi-stationary or time-dependent.

Summarizing [2, 3, 4], we get the derivation of our next formulation. Assuming that the crack C is fully contained in the domain Ω (i.e., it does not reach the boundary) when the elastic energy restitution rate reaches a critical value G_c and following Griffith's criterion leads to the total energy of the crack C which is minimized with respect to the kinematically admissible displacements u and any crack set satisfying a crack growth condition. For the incremental phase-field formulation a regularized crack functional is established and the total energy is replaced by a constitutive dissipation functional for a rate independent fracture process:

$$
\begin{aligned}
E_\epsilon &= \frac{1}{2}\Big(\big((1-\kappa)\varphi^2 + \kappa\big)\sigma(u), e(u)\Big) + G_c\left(\frac{1}{2\epsilon}(1-\varphi)^2 + \frac{\epsilon}{2}|\nabla\varphi|^2\right) \\
&= \int_\Omega \big((1-\kappa)\varphi^2 + \kappa\big)\sigma(u) : e(u)\ dx + G_c\int_\Omega \frac{1}{2\epsilon}(1-\varphi)^2 + \frac{\epsilon}{2}|\nabla\varphi|^2\ dx,
\end{aligned} \tag{3.5}
$$

where the first term characterizes the bulk energy, the second one the surface energy of the crack. Differentiation with respect to the unknowns u and φ, the Euler-Lagrange system for the phase-field fracture reads the equations which we will implement in the numerical example later on:

Formulation 2 *Find a solution $\{u, \varphi\} \in \{u_D + V\} \times W$ such that*

$$\Big(\big((1-\kappa)\varphi^2 + \kappa\big)\sigma^+(u), e(w)\Big) + \big(\sigma^-(u), e(w)\big) = 0 \quad \forall w \in V \tag{3.6}$$

$$
\begin{aligned}
&(1-\kappa)(\varphi\,\sigma^+(u) : e(u), \psi - \varphi) \\
&+ G_c\left(-\frac{1}{\epsilon}(1-\varphi, \psi - \varphi) + \epsilon\big(\nabla\varphi, \nabla(\psi - \varphi)\big)\right) \geq 0 \quad \forall \psi \in W_{in}.
\end{aligned} \tag{3.7}
$$

(3.6) refers to the elasticity part of our system, equation (3.7) is related to the phase-field part. $(\cdot, \cdot)$ stands for the L^2 scalar product and $\cdot : \cdot$ for the scalar product between two matrices. G_c denotes the critical energy release rate and we are using Hook's law for the linear stress-strain-relation:

$$\sigma := \sigma(u) = 2\mu_s e(u) + \lambda_s \, tr \, e(u) \, I, \tag{3.8}$$

where μ_s and λ_s declare the Lamé coefficients and $e(u) = \frac{1}{2}(\nabla u + \nabla u^T)$ constitutes the strain tensor. As in [5], for 2D the stress σ can be splitted into a tensile part σ^+ and a compressive part σ^-:

$$
\begin{aligned}
\sigma^+ &= 2\mu_s e^+ + \lambda_s < tr \, (e) > I \\
\sigma^- &= 2\mu_s (e - e^+) + \lambda_s (tr \, (e) - < tr \, (e) >) I,
\end{aligned}
\tag{3.9}
$$

with

$$e^+ = P \Lambda P^T \tag{3.10}$$

and

$$\Lambda^+ := \Lambda^+(u) := \begin{pmatrix} < \lambda_1(u) & 0 \\ 0 & < \lambda_2(u) \end{pmatrix}. \tag{3.11}$$

Here, $< \cdot >$ declares the positive part of a function, $\lambda_1(u)$ and $\lambda_2(u)$ are the eigenvalues of the strain tensor e with its normalized corresponding eigenvectors $v_1(u)$ and $v_2(u)$. The matrix consisting of the column vectors v_1 and v_2 is defined as $P := P(u) := (v_1, v_2)$. κ is a small positive regularization parameter for the elastic energy residual stiffness of the material. Note, that the material stiffness decreases for approaching the fracture, as

$$\lim_{\varphi \to 0} \left((1 - \kappa)\varphi^2 + \kappa \right) = \kappa. \tag{3.12}$$

Time only occurs indirectly in Formulation 2, i.e., there are no time-derivatives. It may be imported though time-dependent boundary conditions as $u_D = u_D(t) = g(t)$ on ∂B or time-dependent right hand side forces $f(t)$. Furthermore the previous formulation is nonlinear due to the stress splitting, the inequality constraint, the monolithic formulation and the term $(1 - \kappa)(\varphi \, \sigma^+(u) : e(u), \psi - \varphi)$.

3.2   Quasi-monolithic and fully monolithic semi-linear forms

Concerning the non-convexity of the term

$$\big((1-\kappa)\varphi^2 + \kappa\big)\sigma^+(u) \tag{3.13}$$

from Formulation 2 in both unknowns, u and φ, there are sophisticated solution algorithms needed. As shown in [1], one monolithic approach (i.e., all equations are solved simultaneously resulting in one semi-linear form) is based on a linear-in-time extrapolation of φ in (3.6) for the purpose of replacing the 4th-order non-convex term by a given coefficient in front of the elasticity. This new variable is named by $\tilde{\varphi}$ and gives us

$$\big((1-\kappa)\tilde{\varphi}^2 + \kappa\big)\sigma^+(u) \tag{3.14}$$

instead of the above term. This extrapolation is heuristic and robust. The novel problem applying the extrapolated $\tilde{\varphi}$ instead of φ is declared by:

Formulation 3 *Find $U := \{u, \varphi\} \in \{u_D + V\} \times W$ such that*

$$
\begin{aligned}
A(U)(\Psi - U) = \Big(\big((1-\kappa)\tilde{\varphi}^2 &+ \kappa\big)\sigma^+(u), e(w)\Big) + \big(\sigma^-(u), e(w)\big) \\
&+ (1-\kappa)(\varphi\,\sigma^+(u) : e(u), \psi - \varphi) \\
&+ G_c\left(-\frac{1}{\epsilon}(1-\varphi, \psi - \varphi) + \epsilon\big(\nabla\varphi, \nabla(\psi - \varphi)\big)\right) \\
\geq 0 \qquad\qquad &\forall \Psi := \{w, \psi\} \in V \times W_{in}.
\end{aligned}
\tag{3.15}
$$

Remark 1 *We get a fully monolithic semi-linear form by substituting $\tilde{\varphi}$ by φ in the preceded Formulation 3.*

3.3   Temporal and spatial discretization

In this chapter, we first discretize our system in time which gives us an incremental formulation for our quasi-static problem. Therefore we discretize our irreversibility condition (3.3) with a backward difference quotient such that

$$\frac{\varphi - \varphi^{n-1}}{\partial t} \leq 0, \tag{3.16}$$

with

$$\partial t := t^n - t^{n-1} \qquad \text{time step}$$
$$\varphi^{n-1} := \varphi(t^{n-1}) \qquad \text{preceded time step solution}$$
$$\varphi := \varphi^n := \varphi(t^n) \quad \text{current time step sulution.}$$

This leads us to an augmented Lagrangian formulation of (3.3):

$$\varphi \leq \varphi^{n-1} \quad \rightarrow \quad [\Xi + \gamma(\varphi - \varphi^{n-1})]^+, \tag{3.17}$$

where $\Xi \in L^2$ denotes the penalization function which is in general computed by an additional iteration (see [1], Section 4), $\gamma > 0$ and $[x]^+ := max(x, 0)$. Out of this we get:

Formulation 4 *Find $U = \{u, \varphi\} \in \{u_D + V\} \times W$ such that*

$$A(U)(\Psi) := \tilde{A}(U)(\Psi) + [\Xi + \gamma(\varphi - \varphi^{n-1})]^+ = 0 \quad \forall \Psi := \{w, \psi\} \in V \times W, \tag{3.18}$$

where

$$\tilde{A}(U)(\Psi) = \Big(\big((1-\kappa)\tilde{\varphi}^2 + \kappa\big)\sigma^+(u), e(w)\Big) + \big(\sigma^-(u), e(w)\big)$$
$$+ (1-\kappa)(\varphi\,\sigma^+(u) : e(u), \psi) \tag{3.19}$$
$$+ G_c\left(-\frac{1}{\epsilon}(1-\varphi, \psi) + \epsilon\big(\nabla\varphi, \nabla\psi\big)\right).$$

Remark 2 *As in the previous subchapter we obtain the fully monolithic form of Formulation 4 by replacing $\tilde{\varphi}$ by φ.*

Now we discretize Formulation 4 spatially with a discretization parameter h. For this a Galerkin Finite Element scheme is utilized. We refer to Braess [31], Rannacher and Ciarlet [33] for foundations on Finite Elements. Specially for methods on Galerkin Finite Elements we cite Bangerth et al. [30] and Thomée [32].

There are H^1 conforming discrete spaces $V_h \subset V$ and $W_h \subset W$ devoted which consist of bilinear functions Q_1^c on quadrilaterals. The resulting formulation is given by:

Formulation 5 *Find $U_h = \{u_h, \varphi_h\} \in \{u_D^h + V_h\} \times W_h$ such that*

$$A(U_h)(\Psi_h) := \tilde{A}(U_h)(\Psi_h) + [\Xi_h + \gamma(\varphi_h - \varphi_h^{n-1})]^+ = 0 \quad \forall \Psi_h \in V_h \times W_h. \qquad (3.20)$$

For the incremental, spatially discretized problem an adaptive error-oriented Newton algorithm is applied which works as an inner loop within an inexact augmented Lagrangian iteration as shown by Wick [1]. We will take a closer look on it.

To deal with the fully monolithic form of Formulation 5, see also Remark 2, we utilize an error-oriented Newton algorithm as presented in [29], since this approach can cope with highly nonlinear problems and it is based on a natural monotonicity test in which the ordinary Newton update is compared to a simplified one. It has also a higher robustness at the time point when the fracture starts growing.

First, we create the Jacobian matrix by evaluating the directional derivative $A'(U)(\delta U, \Psi)$ with the Newton update $\delta U := \{\delta u, \delta \varphi\} \in V \times W$. For the extrapolated version we get:

$$\begin{aligned}
A'(U)(\delta U, \Psi) = & \left(\left((1-\kappa)\tilde{\varphi}^2 + \kappa \right)\sigma^+(\delta u), e(w) \right) + \left(\sigma^-(\delta u), e(w) \right) \\
& + (1-\kappa)(\delta\varphi\, \sigma^+(u) : e(u) + 2\,\varphi\,\sigma^+(\delta u) : e(u), \psi) \\
& + G_c \left(-\frac{1}{\epsilon}(\delta\varphi, \psi) + \epsilon\big(\nabla\delta\varphi, \nabla\psi\big) \right). \\
& + \gamma(\delta\varphi, \psi)_{A(\varphi)} \qquad\qquad \forall\Psi := w, \psi \in V \times W,
\end{aligned} \qquad (3.21)$$

and for the fully monolithic version:

$$\begin{aligned}
& A'(U)(\delta U, \Psi) \\
& = \left(2\,\delta\varphi(1-\kappa)\varphi\,\sigma^+(u) + \left((1-\kappa)\varphi^2 + \kappa \right)\sigma^+(\delta u), e(w) \right) + \left(\sigma^-(\delta u), e(w) \right) \\
& \quad + (1-\kappa)(\delta\varphi\,\sigma^+(u) : e(u) + 2\,\varphi\,\sigma^+(\delta u) : e(u), \psi) \\
& \quad + G_c \left(-\frac{1}{\epsilon}(\delta\varphi, \psi) + \epsilon\big(\nabla\delta\varphi, \nabla\psi\big) \right). \\
& \quad + \gamma(\delta\varphi, \psi)_{A(\varphi)} \qquad\qquad \forall\Psi := w, \psi \in V \times W,
\end{aligned} \qquad (3.22)$$

where

$$A(\varphi) = \{x = (x_1, x_2) \in B \mid \gamma(\varphi(x) - \varphi(x)^{n-1}) > 0\}. \qquad (3.23)$$

In $\sigma^+(\delta u)$ and $\sigma^-(\delta u)$ we use the derivative of e^+, which is given by

$$e^+(\delta u) = P(\delta u)\Lambda^+ P^T + P\Lambda^+(\delta u)P^T + P\Lambda^+ P^T(\delta u). \tag{3.24}$$

Next, we repeat a classical Newton algorithm, as given in [1], which then will be modified to an error-oriented Newton algorithm. In the following we utilize the discrete norm $\|\cdot\| := \|\cdot\|_{l^2}$.

Algorithm 1 (Residual-based Newton's method) *The main criterion of this method is a decrease of the residual in each step. Estimate an initial Newton value U^0. For $k = 1, 2, 3, \ldots$:*

  1. *Find $\delta U^k := \{\delta u, \delta\varphi\} \in V \times W$ such that*

$$A'(U^k)(\delta U^k, \Psi) = -A(U^k)(\Psi) \quad \forall\Psi \in V \times W,$$
$$U^{k+1} = U^k + \lambda_k\, \delta U^k,$$

  for $\lambda_k = 1$.

  2. *The criterion for convergence is contractions of the residuals:*

$$\|A(U^{k+1})(\Psi)\| < \|A(U^k)(\Psi)\|. \tag{3.25}$$

  3. *If (3.25) is violated, replace U^{k+1} by choosing $\lambda_k^l = 0.5$, and computing for $l = 1, \ldots, l_M$ (e.g., $l_M = 10$) a new solution*

$$U^{k+1} = U^k + \lambda_k^l\, \delta U^k$$

  until (3.25) is fulfilled for a $l^* < l_M$ or l_M is reached. In the second case, no convergence is obtained and the program terminates.

  4. *In case of $l^* < l_M$ we check next the stopping criterion:*

$$\|A(U^{k+1})(\Psi)\| \leq TOL_N.$$

  If this criterion is fulfilled, set $U^* := U^{k+1}$. Else, increment $k \to k+1$ and go to Step 1.

Remark 3 (Quasi-Newton steps) *In order to accelerate Newton's method close to the solution U^*, intermediate quasi-Newton steps are used. For case $\lambda_k = 1$ we take*

$$\theta_k = \frac{\|A(U^{k+1})(\Psi)\|}{\|A(U^k)(\Psi)\|}.$$

If $\theta_k < \theta_{max} < 1$ (e.g., $\theta_{max} \approx 0.1$), then do not build the Jacobian and use the last version that is available.

The error-oriented Newton's algorithm is then given by:

Algorithm 2 (Error-oriented Newton's method) *This method is characterized by a decrease of the norm of the update δU^k. Set $\lambda_{min} \sim 10^{-10}$. Estimate an initial Newton value U^0. For $k = 1, 2, 3, \ldots$:*

1. *Solve for $\delta U^k := \{\delta u, \delta \varphi\} \in V \times W$:*

$$A'(U^k)(\delta U^k, \Psi) = -A(U^k)(\Psi) \quad \forall \Psi \in V \times W.$$

2. *Check if $\|\delta U^k\| \leq TOL_N$. If true, stop and the solution is given by*

$$U^* := U^k + \delta U^k.$$

   Else and if $k > 0$ compute a prediction value for the damping factor:

$$\lambda_k := (1, \mu_k), \quad \mu_k := \frac{\|\delta U^{k-1}\| \cdot \|\delta U^k_{simp}\|}{\|\delta U^k_{simp} - \delta U^k\| \cdot \|\delta U^k\|},$$

   where δU^k_{simp} is available from the previous iteration $k-1$ by solving the simplified system (3.27).

3. *If*

$$\lambda_k < \lambda_{min}$$

   then terminate the program due to convergence failure.

4. If $\lambda_k > \lambda_{min}$ continue and compute the trial iterate

$$U^{k+1} := U^k + \lambda_k \, \delta U^n \qquad (3.26)$$

and evaluate the new residual $A(U^{k+1})(\Psi)$. Solve the simplified linear system using the old Jacobian: Find $\delta U^{k+1} := \{\delta u_{simp}, \delta\varphi_{simp}\} \in V \times W$:

$$A'(U^k)(\delta U^{k+1}_{simp}, \Psi) = -A(U^{k+1})(\Psi) \quad \forall \Psi \in V \times W. \qquad (3.27)$$

5. Compute the monitoring functions:

$$\theta_k := \frac{\|\delta U^{k+1}_{simp}\|}{\|\delta U^k\|}, \quad \theta_k := \frac{0.5\|\delta U^k\|\lambda_k^2}{\|\delta U^{k+1}_{simp} - (1 - \lambda_k)\delta U^k\|}, \quad \lambda'_k := min\left(\mu'_k, \frac{1}{2}\lambda_k\right).$$

6. If $\theta_k < 1$, we have convergence and continue:

(a) If $\lambda'_k = \lambda_k = 1$, check if

$$\|\delta U^{k+1}_{simp}\| \le TOL_N$$

then stop and the solution is given by:

$$U^* := U^{k+1} + \delta U^{k+1}_{simp}.$$

(b) Else accept U^{k+1} (computed in (3.26)) as new iterate. Then increment $k \to k + 1$ and go again to Step 1.

Remark 4 *The linear equation systems of this Newton's method are solved with the direct solver UMFPACK [28].*

Now, we employ an augmented Lagrangian loop to make sure that the inequality constraint is taken care of. At each time t^n, $n \in \mathbb{N}$, the augmented Lagrangian loop generates the outer loop where at each step the Newton solver is assumed.

Algorithm 3 (Augmented Lagrangian loop with error-oriented Newton)
At each t^n, $n = 0, 1, 2, \ldots$ let $\Xi_{h,0}$ be given, e.g., $\Xi_{h,0} = 0$. Moreover, let $\gamma > 0$ be fixed and given for all t^n. At each time t^n iterate for $m = 0, 1, 2, \ldots$:

1. *Given $\Xi_{h,m}$, we seek $U^n_{h,m+1} = \{u^n_{h,m+1}, \varphi^n_{h,m+1}\}$ by solving Formulation 5 with Newton's method via Algorithm 2.*

2. *Update*

$$\Xi_{h,m+1} = [\Xi_{h,m} + \gamma(\varphi_{h,m+1} - \varphi^{n-1}_h)]^+.$$

   Check the stopping criterion

$$\{\|u^n_{h,m+1} - u^n_{h,m}\|, \|\Xi_{h,m+1} - \Xi_{h,m}\|\} \leq TOL_{AL}, \quad TOL_{AL} > 0. \qquad (3.28)$$

3. (a) *If the stopping criterion is satisfied, set $U^n_h := U^n_{h,m^*}$ where m^* is the m that satisfies (3.28).*

   (b) *Else increment $m \to m+1$ and go to Step 1.*

Remark 5 *Algorithm 3 works in the same way by replacing the error-oriented Newton algorithm by the residual-based version. However, the residual-based version only works well with the quasi-monolithic formulation in which φ is extrapolated.*

4 Dynamic phase-field fracture

In this chapter, we extend our quasi-static phase-field system to the dynamic case and study temporal and spatial discretizations of the equations of motion to get a numerical solution. Borden et al. [8] enhance the phase-field model for quasi-static brittle fracture of Miehe et al. [5] to the dynamic case. Their strategy is to extend a functional with the aid of a kinetic energy term. We refer to [9, 10, 11, 12, 13] for additional literature on dynamic fracture.

4.1 Equations

To change our quasi-static phase-field system (3.1) & (3.2) into a dynamic one, we implement time derivatives to it. Our new system reads:

Formulation 6 *Find a vector-valued displacement u and a scalar-valued phase-field variable φ such that*

$$\rho \partial_{tt} u - \varphi \Delta u = f \quad in \ B \tag{4.1}$$

$$\partial_t \varphi + \epsilon \Delta \varphi + \varphi |\nabla u|^2 - \frac{1}{\epsilon}(1 - \varphi) = 0 \quad in \ B \tag{4.2}$$

$$\partial_t \varphi \leq 0 \quad in \ B. \tag{4.3}$$

with associated Dirichlet and Neumann boundary conditions

$$u = g \quad on \ \partial B_D \times I$$

$$\partial_n(\varphi u) = h \quad on \ \partial B_N \times I$$

$$\partial_n \varphi = 0 \quad on \ \partial B \times I,$$

and initial conditions

$$u(\cdot, 0) = u_0 \quad in \ B \times \{0\}$$

$$\partial_t u(\cdot, 0) = v_0 \quad in \ B \times \{0\}$$

$$\varphi(\cdot, 0) = \varphi_0 \quad in \ B \times \{0\}.$$

Analogously as in chapter 3.1, the first equation refers to the elasticity and the second one to the phase-field. The incompressibility inequality constraint remains unchanged. Now system (4.1) & (4.2) is no longer quasi-static, we arrive at a dynamic framework composed of a wave equation and a heat conduction equation.

We briefly summarize Griffith's theory for dynamic brittle fracture in bodies with arbitrary discrete cracks as shown in Borden et al. [8]. Let $\Omega \subset \mathbb{R}^2$ be an arbitrary body with boundary $\partial\Omega$ including a fracture C, see Figure 4.1. $u(x,t) \in \mathbb{R}^2$ again depicts the displacement of a point $x \in \Omega$ at time $t \in [0, T]$ and spatial components of vectors and tensors are indexed by $i, j = 1, 2$. There are time-dependent Dirichlet boundary conditions $u_i(x,t) = g_i(x,t)$ on $\partial\Omega_{g_i} \subseteq \partial\Omega$ and time-dependent Neumann boundary conditions $u_i(x,t) = h_i(x,t)$ on $\partial\Omega_{h_i} \subseteq \partial\Omega$ needed. The 2x2 infinitesimal strain tensor is given by

$$e_{i,j} = u_{(i,j)} = \frac{1}{2}\left(\frac{\partial u_i}{\partial x_j} + \frac{\partial u_j}{\partial x_i}\right), \tag{4.4}$$

the elastic energy density by

$$\psi_e(e) = \frac{1}{2}\lambda e_{ii}e_{jj} + \mu e_{ij}e_{ij}, \tag{4.5}$$

as we assume isotropic linear elasticity. λ and μ describe the Lamé coefficients. The potential energy of the frame is consisting of the sum of the elastic and fracture energy:

$$\Psi_{pot}(u, \Gamma) = \int_\Omega \psi_e(\nabla^s u)\ dx + \int_\Omega G_c\ dx, \tag{4.6}$$

where G_c characterizes once more the critical energy and $\nabla^s : u \to e$ declares the symmetric gradient operator between the displacement field and the strain tensor. There holds the irreversibility condition

$$C(t) \subseteq C(t + \Delta t) \quad \forall \Delta t > 0. \tag{4.7}$$
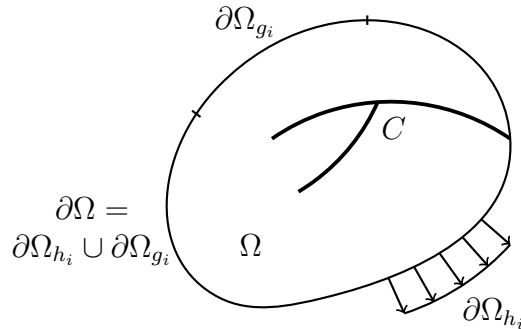

FIG. 4.1: Sample of a solid body Ω including Dirichlet ($\partial\Omega_{g_i}$) and Neumann ($\partial\Omega_{h_i}$) boundary conditions with an initial fracture C.

The potential energy (4.6) of the body together with the kinetic energy

$$\Psi_{kin}(\dot{u}) = \frac{1}{2} \int_\Omega \rho \dot{u}_i \dot{u}_i \ dx, \tag{4.8}$$

where $\dot{u} = \frac{\partial u}{\partial t}$ and ρ presents the mass density of the material, is leading us to the Lagrangian for the discrete fracture problem:

$$
\begin{aligned}
L(u, \dot{u}, C) &= \Psi_{kin}(\dot{u}) - \Psi_{pot}(u, C) \\
&= \int_\Omega \left[\frac{1}{2} \rho \dot{u}_i \dot{u}_i - \psi_e(\nabla^s u) \right] \ dx - \int_C G_c \ dx.
\end{aligned}
\tag{4.9}
$$

We obtain the motion of the body by determining the Euler-Lagrange equations of this functional.

Now we apply this strategy to our system where the fracture C is approximated by a phase-field $\varphi(x, t) \in [0, 1]$, again $\varphi = 0$ indicates the crack region and $\varphi = 1$ the unbroken material. Values between that describe a smooth transition zone depending on a positive regularization parameter ϵ. Next the fracture energy is approximated by

$$\int_C G_c \ dx \approx \int_\Omega G_c \left[\frac{(\varphi - 1)^2}{4\epsilon} + \epsilon \frac{\partial \varphi}{\partial x_i} \frac{\partial \varphi}{\partial x_i} \right] \ dx, \tag{4.10}$$

as Bourdin et al. [14] showed. The elastic energy is approximated by

$$\psi_e(e, \varphi) \approx [(1 - \kappa)\varphi^2 + \kappa]\psi_e^+(e) + \psi_e^-(e) \tag{4.11}$$

and we differentiate between a compressive (i.e. positive) and a tensile (i.e. negative) part of it, see Miehe et al. [5]. This is an important move from a physical point of view, as Borden et al. [8] showed. $\kappa \approx 0$ should be a small positive parameter to inhibit the positive part to vanish in the fully-broken state and for numerical robustness.

Utilize approximations (4.10) & (4.11) in (4.9) leads to the approximation of the Lagrange energy function for the discrete fracture problem in terms of the displacement u and the phase-field approximation of the crack path φ:

$$
\begin{aligned}
L_e(u, \dot{u}, \varphi) &= \int_\Omega \left(\frac{1}{2} \rho \dot{u}_i \dot{u}_i - [(1 - \kappa)\varphi^2 + \kappa]\psi_e^+(\nabla^s u) - \psi_e^-(\nabla^s u) \right) \ dx \\
&\quad - \int_\Omega G_c \left[\frac{(\varphi - 1)^2}{4\epsilon} + \epsilon \frac{\partial \varphi}{\partial x_i} \frac{\partial \varphi}{\partial x_i} \right] \ dx.
\end{aligned}
\tag{4.12}
$$

We calculate the Euler-Lagrange equations of this approximation and receive the strong form equations of motions:

$$\frac{\partial \sigma_{ij}}{\partial x_j} = \rho \ddot{u}_i \quad \text{on } \Omega \times]0, T[\tag{4.13}$$

$$\left(\frac{4\epsilon(1-\kappa)\psi_\epsilon^+}{G_c} + 1 \right) \varphi - 4\epsilon^2 \frac{\partial^2 \varphi}{\partial x_i^2} = 1 \quad \text{on } \Omega \times]0, T[, \tag{4.14}$$

a coupled system of equations that control the motion of the body and evolution of the phase-field. There holds $\ddot{u} = \frac{\partial^2 u}{\partial t^2}$ and the Cauchy stress tensor is given by

$$\sigma_{ij} = [(1-\kappa)\varphi^2 + \kappa]\frac{\partial \psi_e^+}{\partial e_{ij}} + \frac{\partial \psi_e^-}{\partial e_{ij}}. \tag{4.15}$$

Analogous to the derivation of Formulation 2, we get for the dynamic system:

Formulation 7 *Find a solution* $\{u, \varphi\} \in \{u_D + V\} \times W$ *such that*

$$\rho(\partial_{tt}u, w) + \left(\big((1-\kappa)\varphi^2 + \kappa\big)\sigma^+(u), e(w) \right) + \big(\sigma^-(u), e(w)\big) = 0 \quad \forall w \in V \tag{4.16}$$

$$\begin{aligned} &(1-\kappa)(\varphi\,\sigma^+(u) : e(u), \psi - \varphi) \\ &+ G_c \left(\frac{1}{\epsilon}(1-\varphi, \psi - \varphi) + \epsilon\big(\nabla\varphi, \nabla(\psi - \varphi)\big) \right) \geq 0 \quad \forall \psi \in W_{in}, \end{aligned} \tag{4.17}$$

which will be implemented in our code for the example in the next chapter.

4.2   Time stepping

For a numerical reason (see, e.g., [16]) we split the wave equation (4.1), a second order partial differential equation in time, into a first order system in time:

$$\rho\,\partial_t v - \varphi\Delta u = f \tag{4.18}$$

$$\rho(\partial_t u - v) = 0. \tag{4.19}$$

This mixed form of elasticity will be treated for time-stepping schemes below where we work with One-Step-θ schemes.

4.2.1   Basics on One-Step-θ schemes

First, we briefly show the derivation of One-Step-θ schemes, as for example shown in [17, 18, 19]. We consider a parabolic problem like the heat equation

$$\partial_t u - \Delta u = f. \tag{4.20}$$

Time discretization yields:

Find $u := u^n$ such that

$$\frac{u - u^{n-1}}{\delta t} - \theta \Delta u - (1 - \theta)\Delta u^{n-1} = \theta f + (1 - \theta)f^{n-1}, \tag{4.21}$$

hence

$$u - \delta t\, \theta \Delta u = u^{n-1} + \delta t(1 - \theta)\Delta u^{n-1} + \delta t\, \theta f + \delta t(1 - \theta)f^{n-1}. \tag{4.22}$$

Remark 6 *Traditionally time-dependent problems are discretized with the method of lines where first spatial and then temporal discretization is accomplished. This results in an ODE (ordinary differential equations) system which can be solved by standard methods.*

Next we show different time-stepping schemes by the choice of θ.

Definition 1 *(Choice of θ) The following time-stepping schemes are given by the choice of θ:*

- *$\theta = 0$: 1st order explicit Euler time-stepping;*

- *$\theta = 0.5$: 2nd order Crank-Nicolson (trapezoidal rule) time-stepping;*

- *$\theta = 0.5 + k_n$: 2nd order shifted Crank-Nicolson which is shifted by the time step size k towards the implicit side;*

- *$\theta = 1$: 1st order implicit Euler time-stepping.*

For stability properties like numerical stability, absolute stability and A-stability we refer to [17].

4.2.2   One-step-θ time-stepping for the mixed form of elasticity

Here, we apply a One-Step-θ scheme to the mixed form of elasticity, (4.18) & (4.19), leading to

Formulation 8 *Let u^{n-1}, v^{n-1} be given. Find u and v such that:*

$$\rho\, v - \delta t\, \theta \varphi \Delta u = \rho v^{n-1} + \delta t(1-\theta)\Delta u^{n-1} + \delta t\, \theta f + \delta t(1-\theta)f^{n-1} \qquad (4.23)$$

$$u - \delta t\, \theta\, v = u^{n-1} + \delta t(1-\theta)v^{n-1}. \qquad (4.24)$$

4.3   Temporal discretization

Using an extrapolation, as in chapter 3.2, and a penalization, as in chapter 3.3, we get:

Formulation 9 *Find $U = \{u, \varphi\} \in \{u_D + V\} \times W$ such that*

$$A(U)(\Psi) := \tilde{A}(U)(\Psi) + [\Xi + \gamma(\varphi - \varphi^{n-1})]^+ = 0 \quad \forall \Psi := \{w, \psi\} \in V \times W, \qquad (4.25)$$

where

$$\begin{aligned}
\tilde{A}(U)(\Psi) &= \rho(\partial_{tt}u, w) + \Big(\big((1-\kappa)\tilde{\varphi}^2 + \kappa\big)\sigma^+(u), e(w)\Big) \\
&\quad + \big(\sigma^-(u), e(w)\big) + (1-\kappa)(\varphi\, \sigma^+(u) : e(u), \psi) \\
&\quad + G_c\left(-\frac{1}{\epsilon}(1-\varphi, \psi) + \epsilon\big(\nabla\varphi, \nabla\psi\big)\right).
\end{aligned} \qquad (4.26)$$

Remark 7 *As bevor, we obtain the fully monolithic form of this formulation by replacing $\tilde{\varphi}$ by φ.*

For numerical calculations we can convert the weak formulation of the dynamic phase-field system into a first-order system and make use of One-Step-θ schemes: splitting the elasticity equation from Formulation 7, the dynamic phase-field fracture reads:

Formulation 10 *Find a solution $\{v, u, \varphi\} \in L \times \{u_D + V\} \times W$ such that*

$$\rho(\partial_t v, w) + \left(\left((1 - \kappa)\varphi^2 + \kappa \right) \sigma^+(u), e(w) \right) + \left(\sigma^-(u), e(w) \right) = 0 \quad \forall w \in V \qquad (4.27)$$

$$\rho(\partial_t u - v, w) = 0 \quad \forall w \in L \qquad (4.28)$$

$$(1 - \kappa)(\varphi\, \sigma^+(u) : e(u), \psi - \varphi)$$
$$+ G_c \left(\frac{1}{\epsilon}(1 - \varphi, \psi - \varphi) + \epsilon\left(\nabla\varphi, \nabla(\psi - \varphi) \right) \right) \geq 0 \quad \forall \psi \in W_{in}. \qquad (4.29)$$

Now applying the One-Step-θ scheme on the elasticity equation results in:

Formulation 11 *Let u^{n-1}, v^{n-1} be given. Find $u, v \in \{u_D + V\} \times L$ such that:*

$$\rho\left(\frac{v - v^{n-1}}{\delta t}, w \right) + \theta\left(\left((1 - \kappa)\varphi^2 + \kappa \right)\sigma^+(u), e(w) \right)$$
$$+ (1 - \theta)\left(\left((1 - \kappa)\varphi^2 + \kappa \right)\sigma^+(u^{n-1}), e(w) \right) \qquad (4.30)$$
$$+ \theta\left(\sigma^-(u), e(w) \right) + (1 - \theta)\left(\sigma^-(u^{n-1}), e(w) \right) = 0 \quad \forall w \in V$$

$$\rho\left(\frac{u - u^{n-1}}{\delta t}, w \right) - \theta\rho(v, w) - (1 - \theta)\rho(v^{n-1}, w) = 0 \quad \forall w \in L. \qquad (4.31)$$

4.4 Spatial discretization

After time discretization, we discretize Formulation 9 with a spatial discretization parameter h. For this a Galerkin finite element scheme is utilized as in the quasi-static case. There are again H^1 conforming discrete spaces $V_h \subset V$ and $W_h \subset W$ devoted which consist of bilinear functions Q_1^c on quadrilaterals. The resulting formulation is given by:

Formulation 12 *Find $U_h = \{u_h, \varphi_h\} \in \{u_D^h + V_h\} \times W_h$ such that*

$$A(U_h)(\Psi_h) := \tilde{A}(U_h)(\Psi_h) + [\Xi_h + \gamma(\varphi_h - \varphi_h^{n-1})]^+ = 0 \quad \forall \Psi_h \in V_h \times W_h. \qquad (4.32)$$

Having the saptial discretization in abstract form given in (12), we obtain the fully discretized system by adding formally h into (4.30) and (4.31). Then:

Formulation 13 *Let u_h^{n-1}, v_h^{n-1} be given. Find $u_h, v_h \in \{u_D^h + V_h\} \times L_h$ such that:*

$$\rho\left(\frac{v_h - v_h^{n-1}}{\delta t}, w_h\right) + \theta\Big(\big((1-\kappa)\varphi^2 + \kappa\big)\sigma^+(u_h), e(w_h)\Big)$$
$$+ (1-\theta)\Big(\big((1-\kappa)\varphi^2 + \kappa\big)\sigma^+(u_h^{n-1}), e(w_h)\Big) \tag{4.33}$$
$$+ \theta\big(\sigma^-(u_h), e(w_h)\big) + (1-\theta)\big(\sigma^-(u_h^{n-1}), e(w_h)\big) = 0 \quad \forall w_h \in V_h$$

$$\rho\left(\frac{u_h - u_h^{n-1}}{\delta t}, w_h\right) - \theta\rho(v_h, w_h) - (1-\theta)\rho(v_h^{n-1}, w_h) = 0 \quad \forall w_h \in L_h. \tag{4.34}$$

5 Numerical tests (Single edged notched shear test)

In this final chapter, we investigate the numerical performance of the phase-field fracture model. We study numerical tests in 2D based on the single edged notched shear test, as given in [1, 5], where we compare the quasi-static and the dynamic fracture model in case of accuracy and computational costs using different time-stepping schemes. Therefore we take a look at the load-displacement curves, the Newton convergence and the crack patterns for our formulations.

5.1 Configuration of the single edged notched shear test

In our example, we observe, as in [1, 5], a pure elastic crack-propagation sample in order to unstable and brutal crack growth. The single edge notched shear test we look at, is based on a self-developed code in the finite element software deal.II [6] by Thomas Wick [27] which is examined and modified in this thesis.

As shown in Figure 5.1, we consider a squared plate involving a horizontal notch at the middle height from the right boundary to the center of the specimen. The boundary conditions are defined through $u_y = 0$ mm and traction-free (i.e., the surface is free from external stress) in x-direction on the left as well as on the right side of the sample. On the bottom part there holds $u_x = u_y = 0$. Further we get $u_y = 0$ mm and a time-dependent non-homogeneous Dirichlet condition $u_x = t\bar{u}$, $\bar{u} = 1$ mm/s on $\Gamma_{top} := \{(x, y) \in B \mid 0 \text{ mm} \leq x \leq 10 \text{ mm}, \ y = 10 \text{ mm}\}$ due to the increased displacement over time t. On the lower part of the slit we obtain $u_y = 0$ mm.
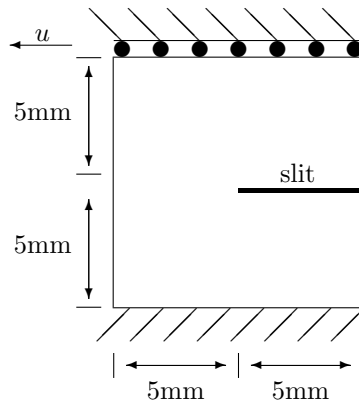
FIG. 5.1: The configuration of the single edge notched shear test is given by a squared plate involving a horizontal notch.

It is also important to deal with the spectral decomposition of the stress σ into a tensile part $\sigma^+(u)$ and a compressive part $\sigma^-(u)$ as pointed out in system (3.9). The physical motivation behind that is given by Miehe et al. [5, 7]. In an isotropic model the stress degradation influences the full stress tensor whereby energy is set free based on the fracture in both, tension and compression. As a consequence only implementations with tensile stresses are feasible which is physically unrealistic. This problem can be overcome by decomposing the strain tensor ϵ into a positive and negative part describing the tensile and compressive modes. Based on that, an anisotropic energy storage function (again with a positive and negative part) is defined. The energy storage function describes the energy stored in the mass of the solid per unit volume. The evolution of free energy is then governed by expressions for the energetic force and the stress tensor. In contrast to the isotropic case, where the energetic force is strictly negative, it is now associated to the positive part of the energy. The stress tensor is currently given by a decomposition of the fictitious undamaged solid. As a result the stress degradation is solely influenced by the positive and therefore the tensile part of the stress tensor σ.

The initial mesh is 4 times uniformly refined having 1024 mesh cells with $h = 0.044$ mm. Next we set the parameters. The Lamé coefficients are given by $\mu = 80.77$ kN/mm^2 and $\lambda = 121.15$ kN/mm^2, the critical energy release rate by $G_c = 2.7$ N/mm. $\partial t = 10^{-4}$s denotes the time step size which will be varied in our example, the tolerance of the augmented Lagrangian loop is set to $TOL_{AL} = 10^{-5}$. The regularization parameters are chosen to $\kappa = 10^{-12}$ and $\epsilon = 2h$.

We interpret the surface load vector on Γ_{top} as

$$\tau = (F_x, F_y) := \int_{\Gamma_{top}} \sigma(u)n \ ds, \tag{5.1}$$

where n denotes the normal vector.

5.2 Load-displacement curves for the quasi-static formulation

First we consider the load-displacement curves for the quasi-static case. Therefore we first explain what this curves mean. A load-displacement curve is consisting of the displacement of the boundary versus the stresses in x-direction. The increasing force on the top of the specimen does not immediately lead to the fracture propagation. Due to this, the elastic energy in the sample is rising as well as the shear stress at the top of the boundary. Once the crack spreads out, a part of the elastic energy is converted into crack energy. Thus the stress in x-direction on top of the boundary decreases, including that the "load F_x"-curve is falling.

In Figure 5.2 the load-displacement curves in terms of a backward Euler (BE) and a Crank-Nicolson (CN) scheme are depicted, where we used different time step sizes. We can confirm that an effective element size of $h \approx 0.001$mm is needed for both, backward Euler and Crank-Nicolson, as Miehe et al. [5] showed. All in all we get the same behavior for the load-displacement curves as presented in [1]. We can observe convergence in both cases for our chosen time step sizes.

5.3 Load-displacement curves for the dynamic formulation

In Figure 5.3 we take a look at the load-displacement curves for dynamic fracture. Here, also an effective element size of $h \approx 0.001$mm for both time-stepping schemes is required, as indicated in the previous subchapter.

We get a completely different performance of the load-displacement curves compared to the quasi-static case in both time-stepping schemes, backward Euler and Crank-Nicolson. We do not get the typical behavior of the load-displacement curves as depicted in the preceding subchapter. Out of this curves we can not infer the time where the crack starts to spread out. Now, the energies are distributed in another way as in the quasi-static case. The curves show an oscillating behavior: first they increase rapidly before they collapse at a very early time point, then they again rise and fall.
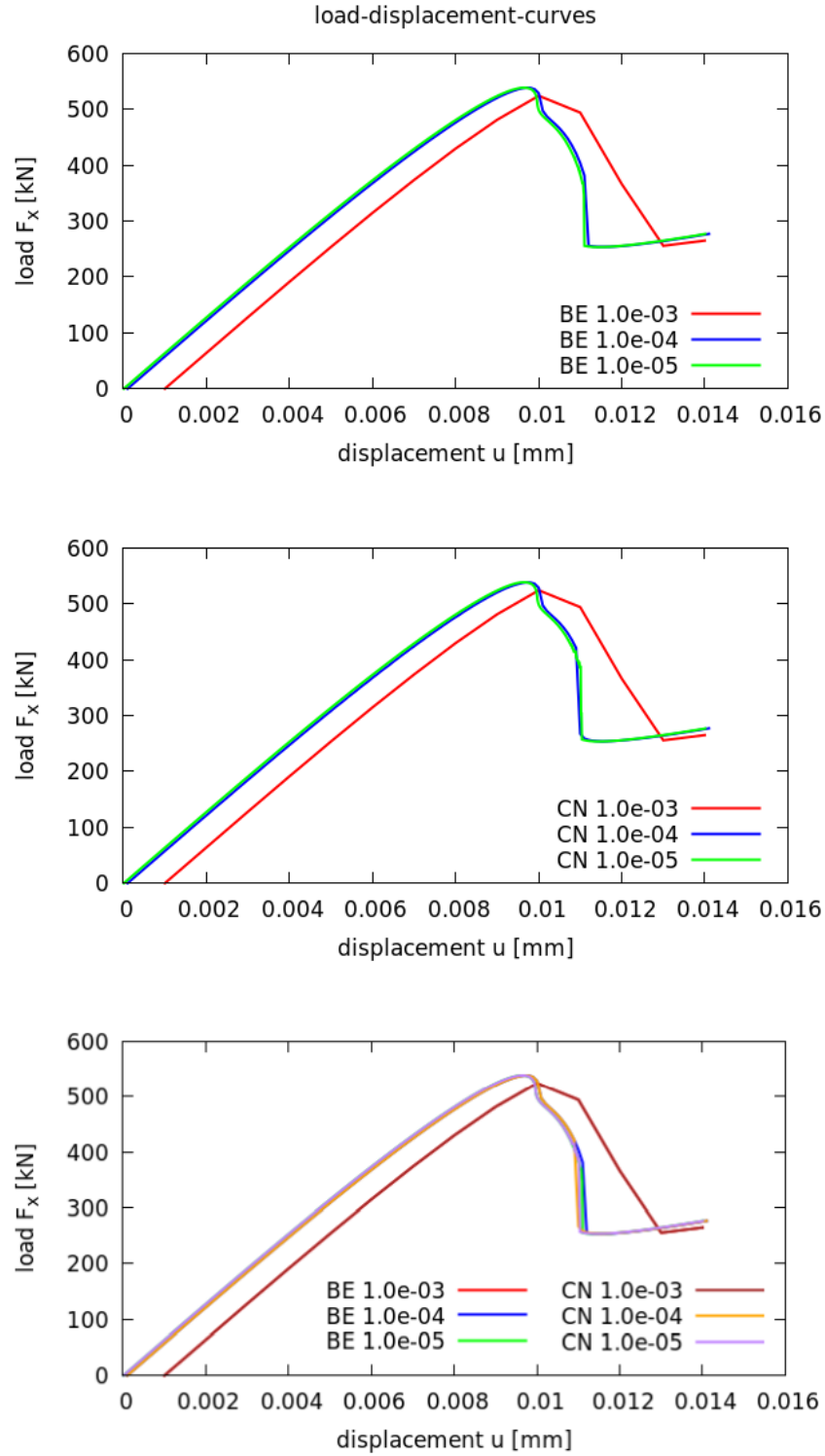
FIG. 5.2: Load-displacement-curves for the quasi-static single edge notched shear test based on a backward Euler (top) and a Crank-Nicolson (middle) time-stepping scheme with different time step sizes. The last picture shows the relation between them.
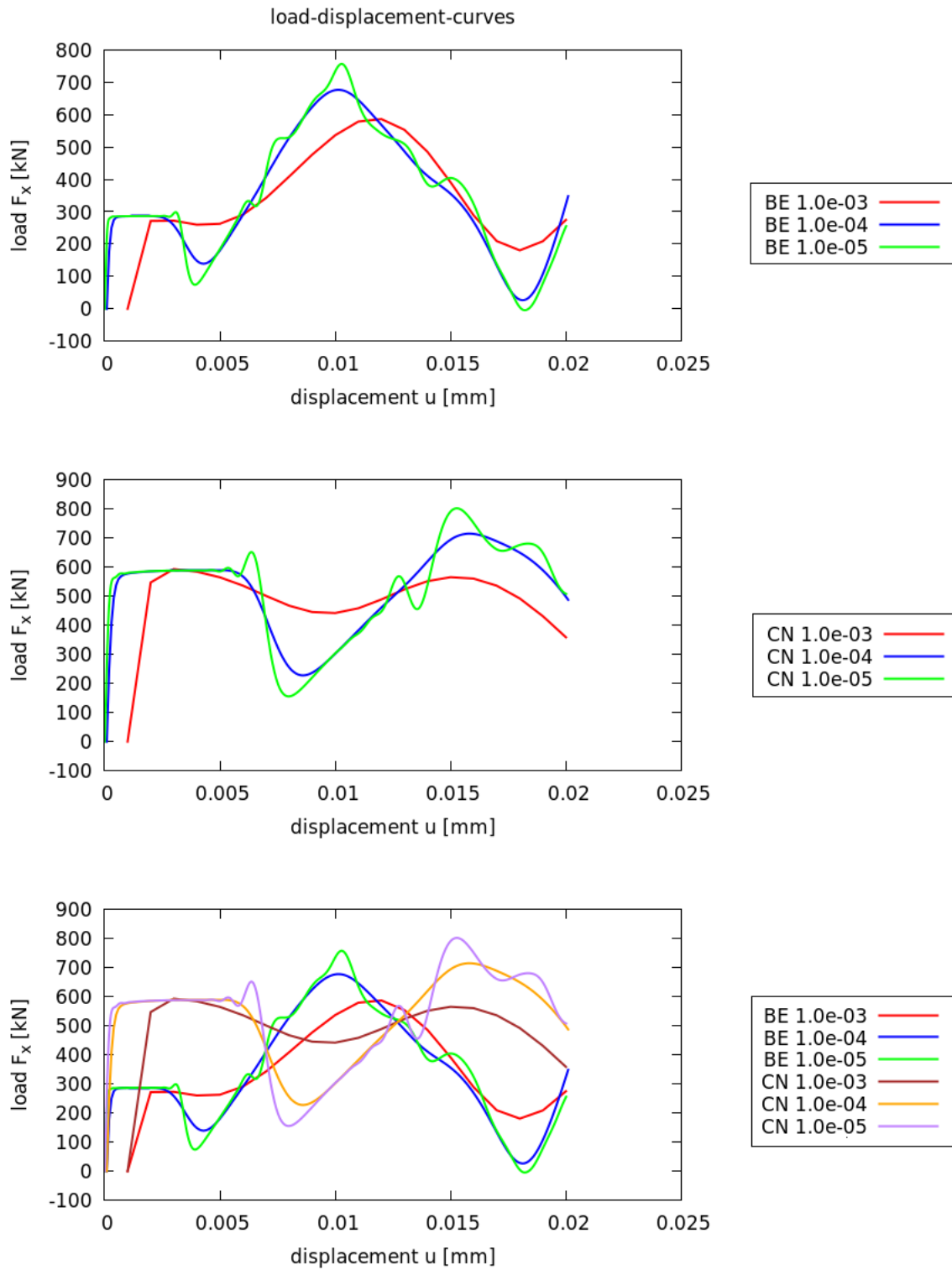
FIG. 5.3: Load-displacement-curves for the dynamic single edge notched shear test based on a backward Euler (top) and a Crank-Nicolson (middle) time-stepping scheme with different time step sizes. The last picture shows the relation between them.

5.4   Newton convergence for the quasi-static formulation

Figure 5.4 exhibit the number of Newton iterations per step for our two time-stepping schemes, backward Euler and Crank-Nicolson, based on different time step sizes in the quasi-static case. Up to the time where the fracture starts growing, we can observe numbers of Newton iterations between 2 and 11. The range gets lesser for smaller time step sizes. For times where the fracture grows there is a highly increase of Newton steps for certain time step sizes. The smaller the time step size the bigger the peak of the number of Newton iterations. This manner could also be determined in [1, 34].

For almost all tests there have augmented Lagrangian iterations been needed to reach the tolerances. For our biggest time step size δt=1.0e-03 using backward Euler, there were up to 5 Lagrangian iterations required. For smaller time step sizes there were up to 2 Lagrangian iterations needed. Nearly the same behavior was observable utilizing Crank-Nicolson.

Looking at table 2, we can see that the (absolute) stopping criterion for Newton's method in this test is given by 1.0e-08. We can observe, that the Newton solver first converges very slow, fast convergence is only given in the last steps. Even in the convergence radius, the Jacobian matrix has to be re-build. Considering the same assumptions using smaller time step sizes we get tables 3 & 4, the configuration yields much faster convergence and the Jacobian matrix has to be build less often. This behavior is in agreement with [17]. The same observations can be made using Crank-Nicolson.

ITER	NEWTON RESIDUAL	JACOBIAN RE-BUILD
1	8.06461e-02	r
2	1.35771e-01	r
3	3.97607e-02	r
4	1.49888e-04	
5	4.14938e-07	
6	6.88425e-08	r
7	2.73926e-08	r
	9.07996e-09	

Table 2: Newton convergence at time step 2 with δt=1.0e-03s using a backward Euler scheme.
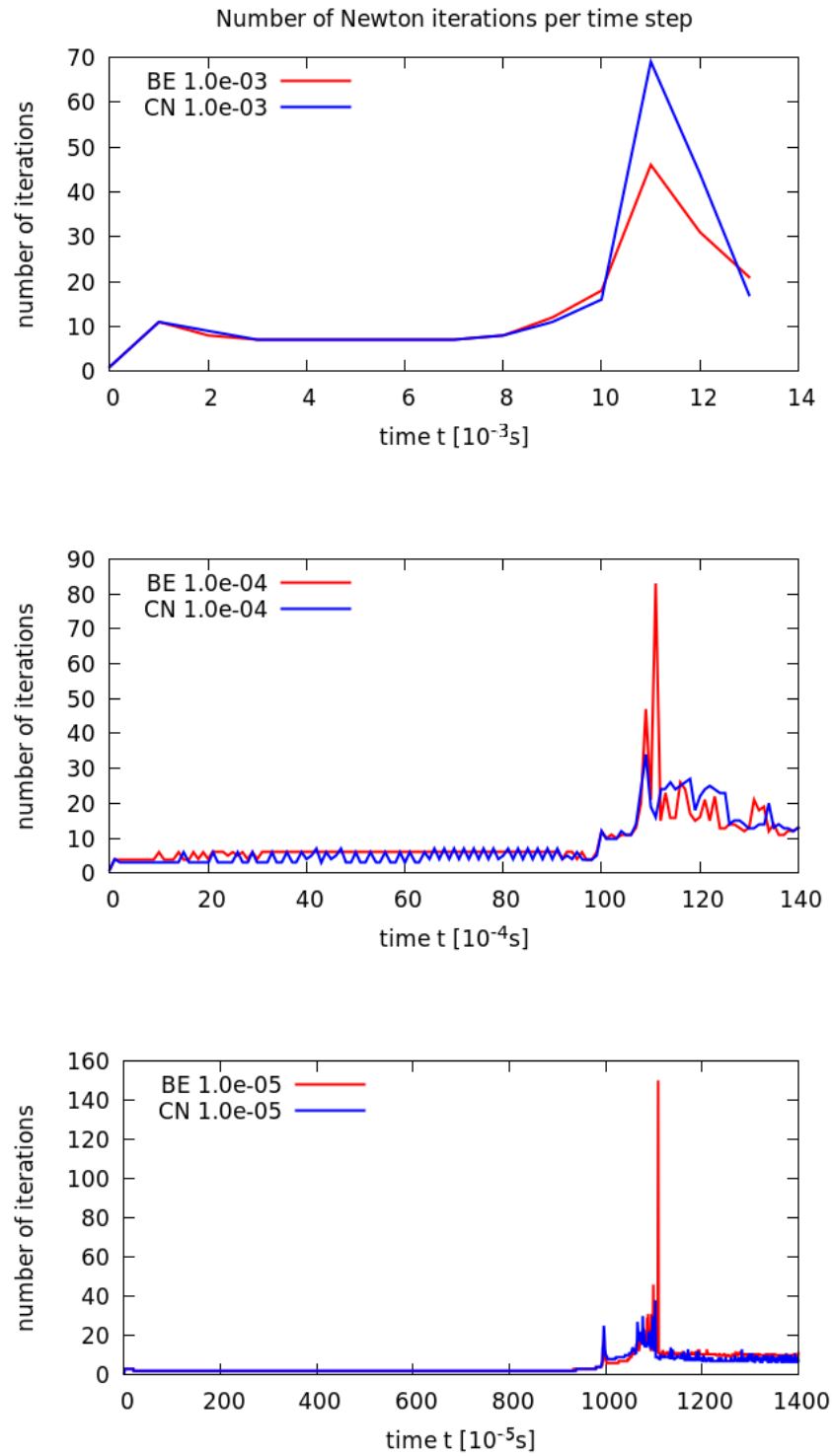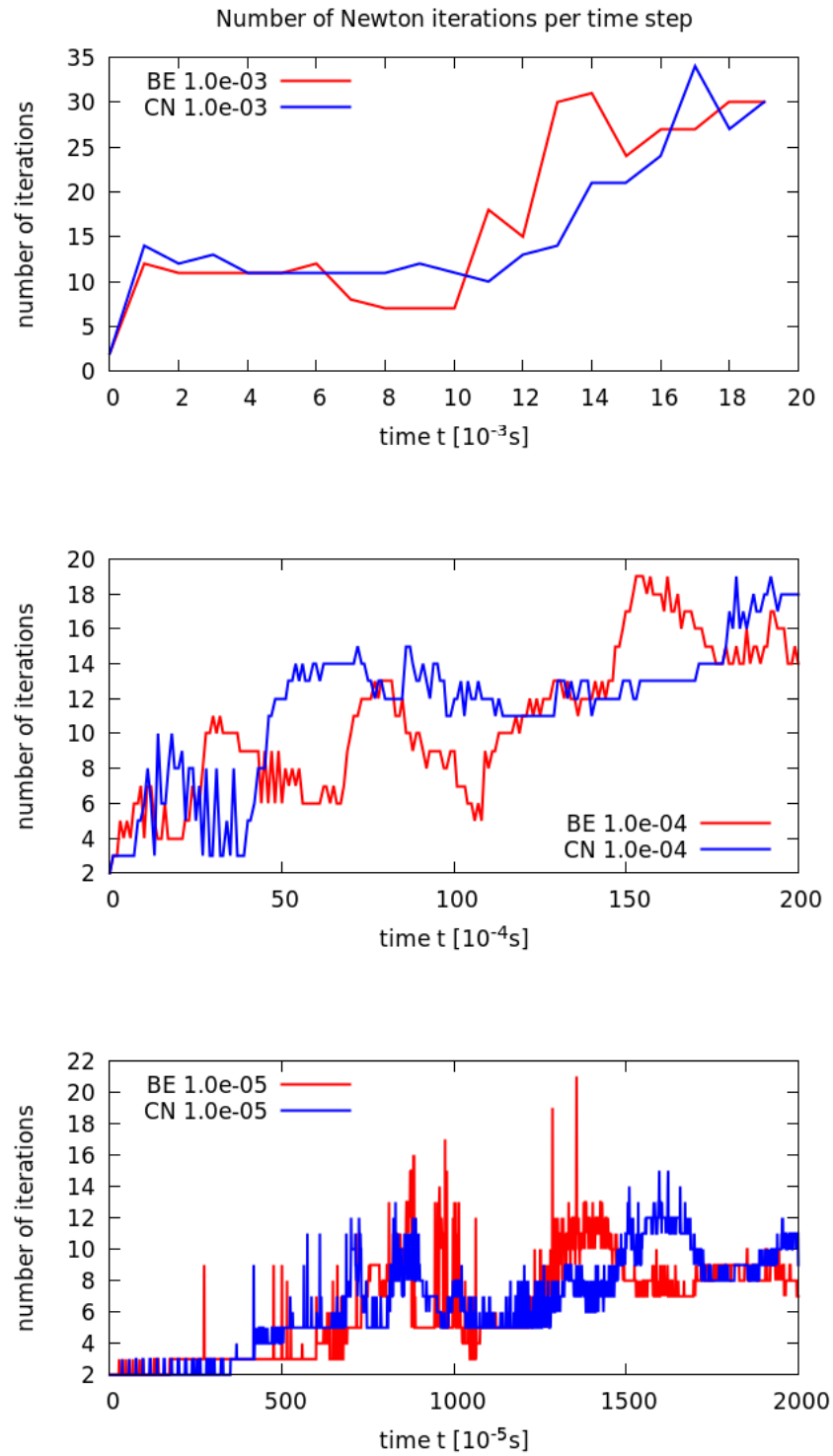
FIG. 5.4: Number of Newton iterations per step for the quasi-static single edge notched shear test in comparison of a backward Euler and a Crank-Nicolson time-stepping scheme with different time step sizes.

ITER	NEWTON RESIDUAL	JACOBIAN RE-BUILD
1	8.05995e-04	r
2	2.98861e-06	
3	1.74371e-08	
	5.96550e-09	

Table 3: Newton convergence at time step 20 with δt=1.0e-04s using a backward Euler scheme.

ITER	NEWTON RESIDUAL	JACOBIAN RE-BUILD
1	8.05880e-06	r
	3.15451e-10	

Table 4: Newton convergence at time step 200 with δt=1.0e-05s using a backward Euler scheme.

5.5   Newton convergence for the dynamic formulation

Next, we regard the number of Newton iterations per step for the dynamic fracture model in Figure 5.5. Again we take a backward Euler and a Crank-Nicolson scheme, depending on different time step sizes. Here, we are not able to observe big differences of the number of Newton iterations in case of the unbroken and the fractured time. All of our three chosen time step sizes yield nearly the same maximum of Newton iteration steps.

For almost all tests there have augmented Lagrangian iterations been needed to reach the tolerances. For the biggest time step size δt=1.0e-03 for both time-stepping schemes, backward Euler and Crank-Nicolson, there were up to 10 Lagrangian iterations required. For smaller time step sizes there were up to 4 Lagrangian iterations needed.

The (absolute) stopping criterion for Newton's method is again given by 1.0e-08. The configuration yields much faster convergence and the Jacobian matrix has to be build less often, as in the quasi-static case. The same observations can be made using Crank-Nicolson.

FIG. 5.5: Number of Newton iterations per step for the dynamic single edge notched shear test based on a backward Euler and a Crank-Nicolson time-stepping scheme with different time step sizes.

5.6   Comparison of quasi-static and dynamic formulations

This subchapter shows the differences of quasi-static and dynamic fracture models.

First, we look at the numerical solutions of the crack patterns (i.e., the phase-field variable). Therefore, we first examine Figure 5.6 which shows the quasi-static progression of the crack in case of a backward Euler scheme for time step size $\delta t=1.0e\text{-}04s$. The fracture starts at time $T=9.8e\text{-}03s$, grows and finally cuts up the whole domain at time $T=1.12e\text{-}02s$. This is in good agreement to [8, 5].

In Figure 5.7 the comparison of the crack patterns for the quasi-static and dynamic fracture model in terms of a backward Euler scheme for different points in time are exposed. Figure 5.8 exhibits this comparison for a Crank-Nicolson scheme. All in all comparing the dynamic with the quasi-static case, we find out that the crack grows slower using dynamic fracture. Therefore we showed the propagation of the crack for dynamic fracture in Figure 5.9 in case of backward Euler and in Figure 5.10 in case of Crank-Nicolson.

Next, we consider the load-displacement curves for the quasi-static and the dynamic case with different time step sizes in Figure 5.11. In the first picture we can see a backward Euler scheme, the second one shows Crank-Nicolson. It is difficult to compare this curves together because we get an oscillating behavior for the dynamic fracture model as already shown in subchapter 5.3.

Looking at Figure 5.12 we can see the number of Newton iterations per time step for quasi-static and dynamic fracture again in terms of a backward Euler and a Crank-Nicolson scheme. The number of Newton iterations is obviously higher using the quasi-static model. For both models the number of Lagrangian iterations is larger for bigger time step sizes, lesser for smaller time step sizes. However this number of iterations is a little bit higher using the dynamic fracture model. The smaller the time step sizes, the better the convergence. Also the Jacobian matrix has to be build less often. This observations holds for both time-stepping schemes.
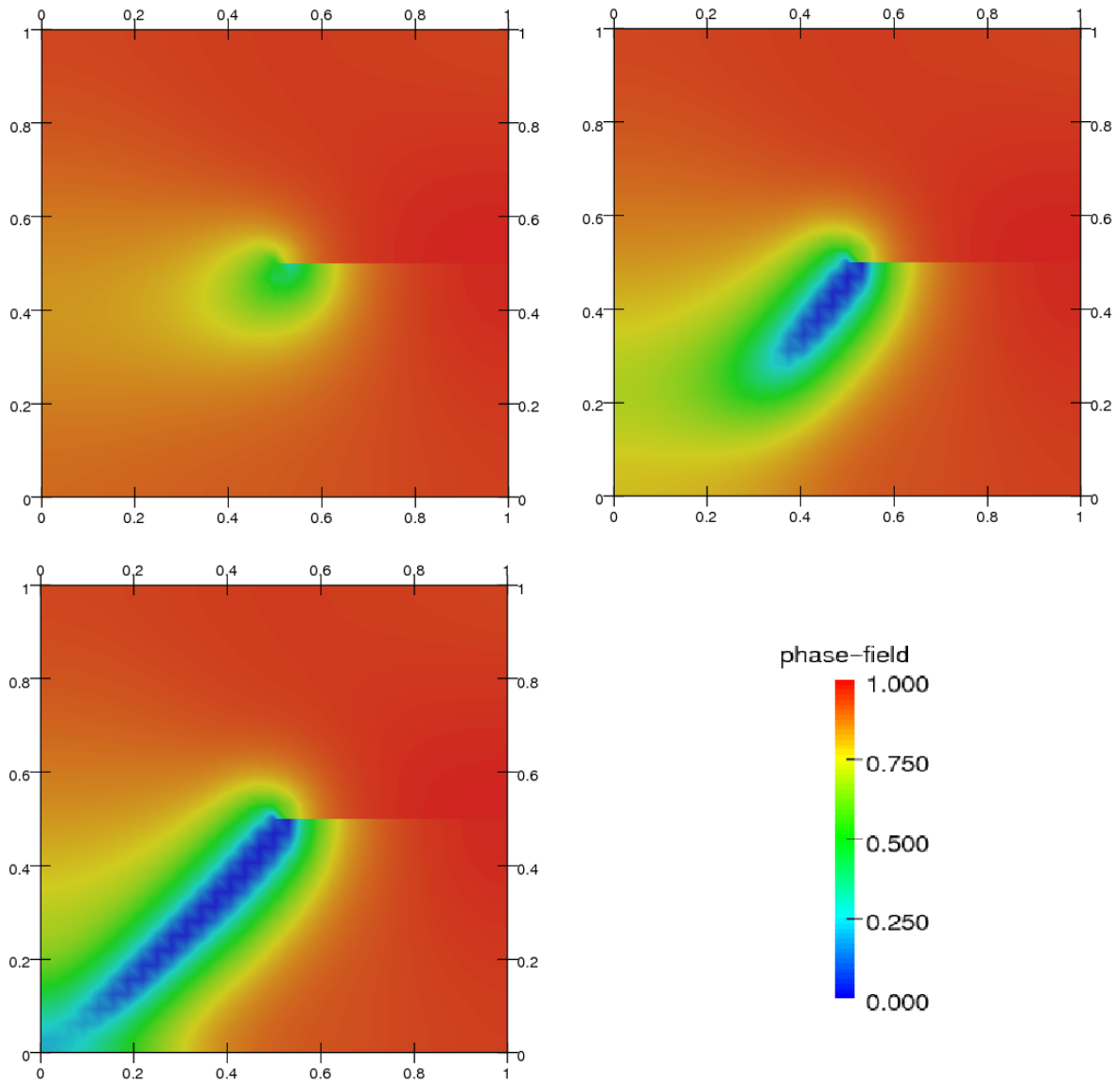
Fig. 5.6: Crack pattern for the quasi-static single edge notched shear test based on a backward Euler scheme for time step size ∂t=1.0e-04s. The upper left picture shows the beginning of the fracture at time T=9.8e-03s, the upper right one the growth of it. In the illustration at the bottom part the crack has cut up the whole domain at time T=1.12e-02s.
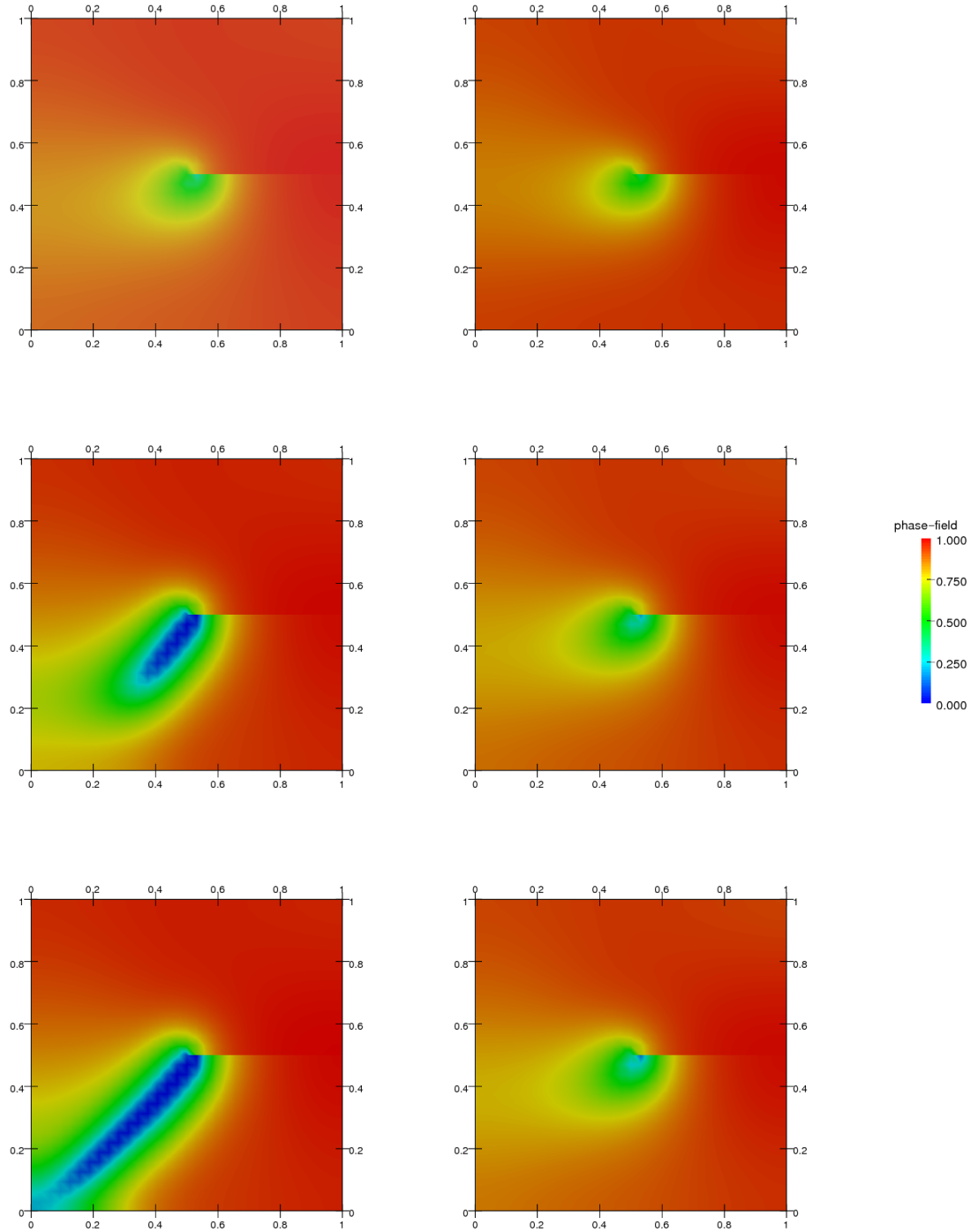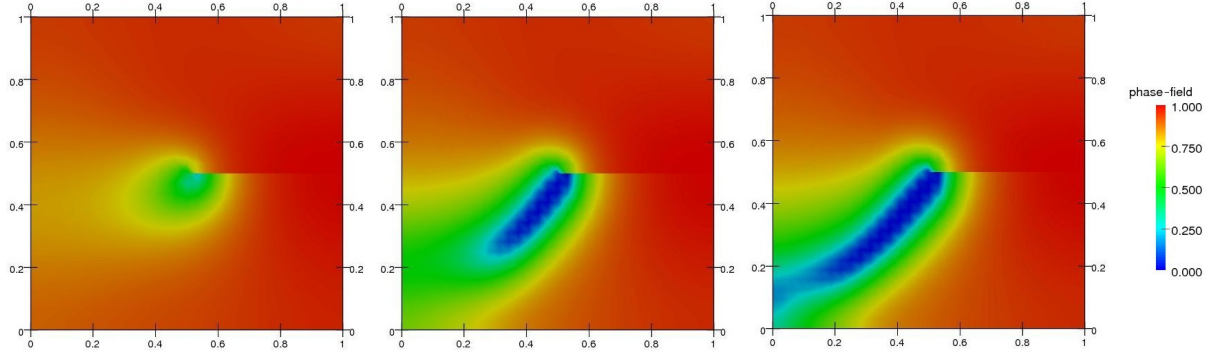
FIG. 5.7: Crack pattern for the quasi-static (left) and dynamic (right) single edge notched shear test based on a backward Euler scheme for time step size ∂t=1.0e-04s. Top: Time T=9.8e-03s, Middle: Time T=1.1e-02s, Bottom: Time T=1.12e-02s.
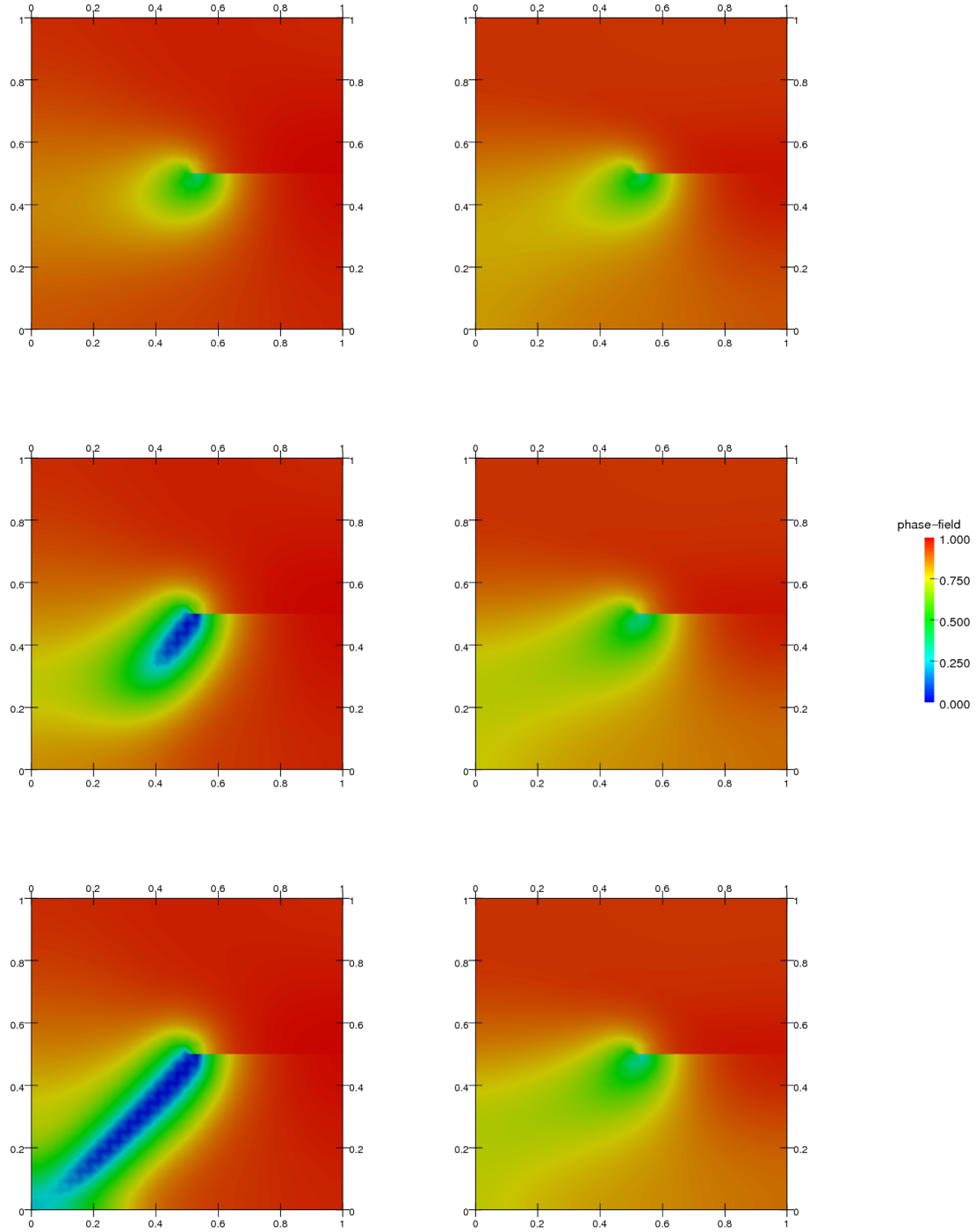
FIG. 5.8: Crack pattern for the quasi-static (left) and dynamic (right) single edge notched shear test based on a Crank-Nicolson scheme for time step size ∂t=1.0e-04s. Top: Time T=9.8e-03s, Middle: Time T=1.08e-02s, Bottom: Time T=1.1e-02s.

FIG. 5.9: Crack pattern for the dynamic single edge notched shear test based on a backward Euler scheme for time step size ∂t=1.0e-04s. Left: Time T=1.09e-02s, Middle: Time T=1.36e-02s, Right: Time T=1.44e-02s.
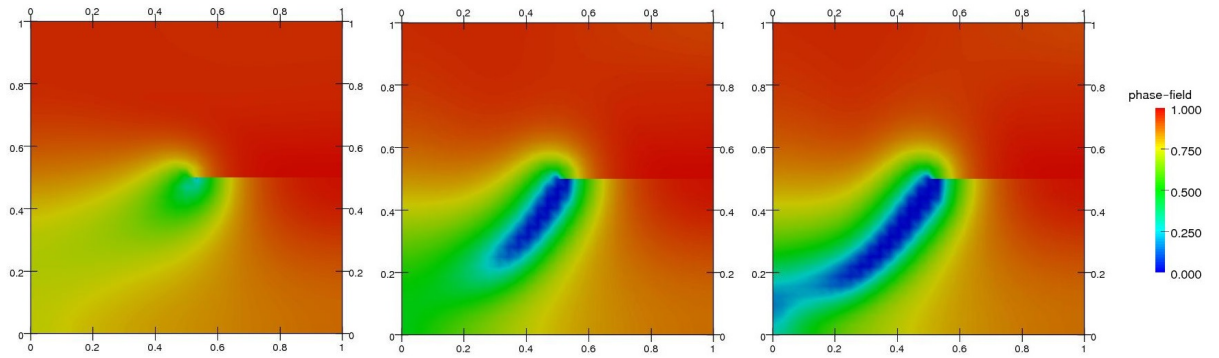
FIG. 5.10: Crack pattern for the dynamic single edge notched shear test based on a Crank-Nicolson scheme for time step size ∂t=1.0e-04s. Left: Time T=1.12e-02s, Middle: Time T=1.54e-02s, Right: Time T=1.70e-02s.
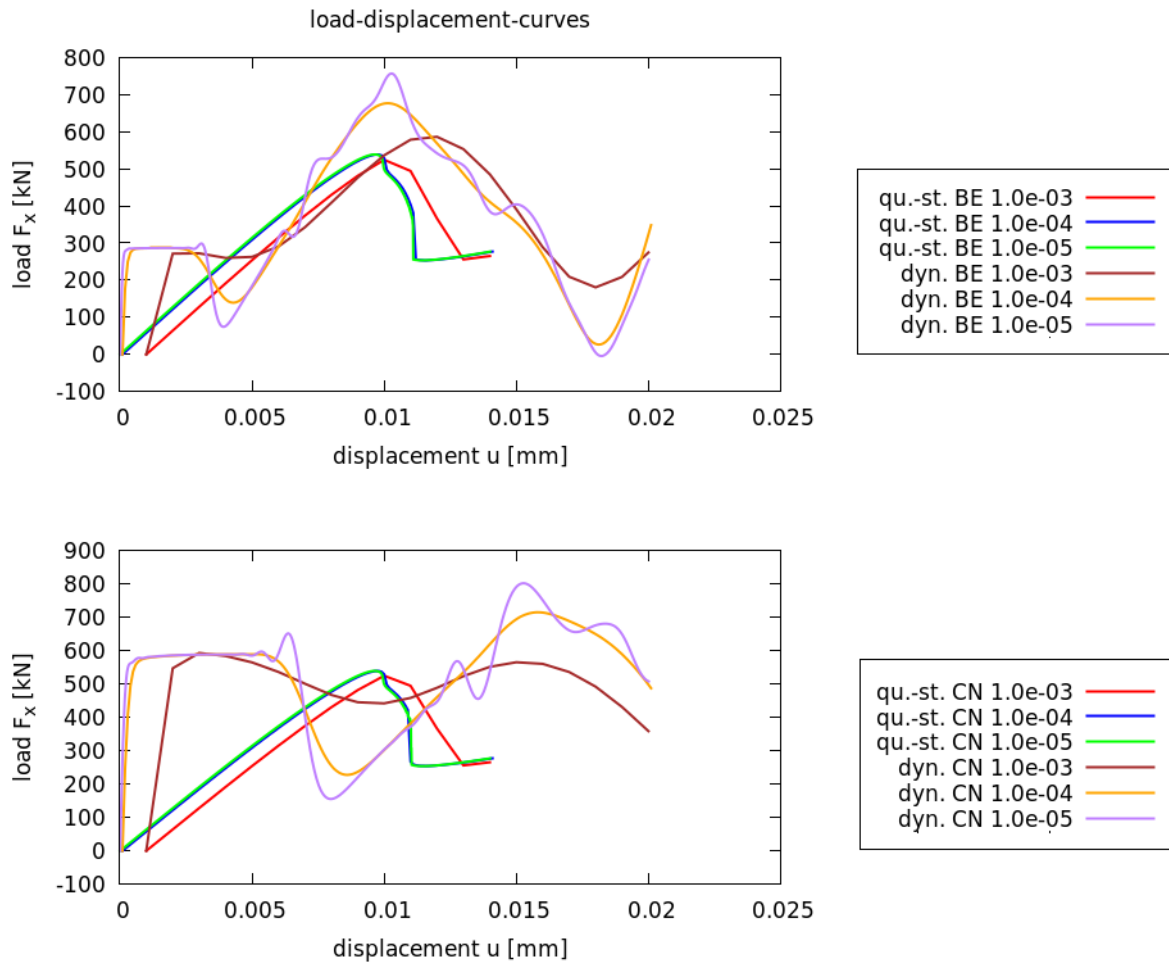
FIG. 5.11: Comparison of the load-displacement curves for the quasi-static and dynamic single edge notched shear test based on a backward Euler and a Crank-Nicolson time-stepping scheme with different time step sizes.
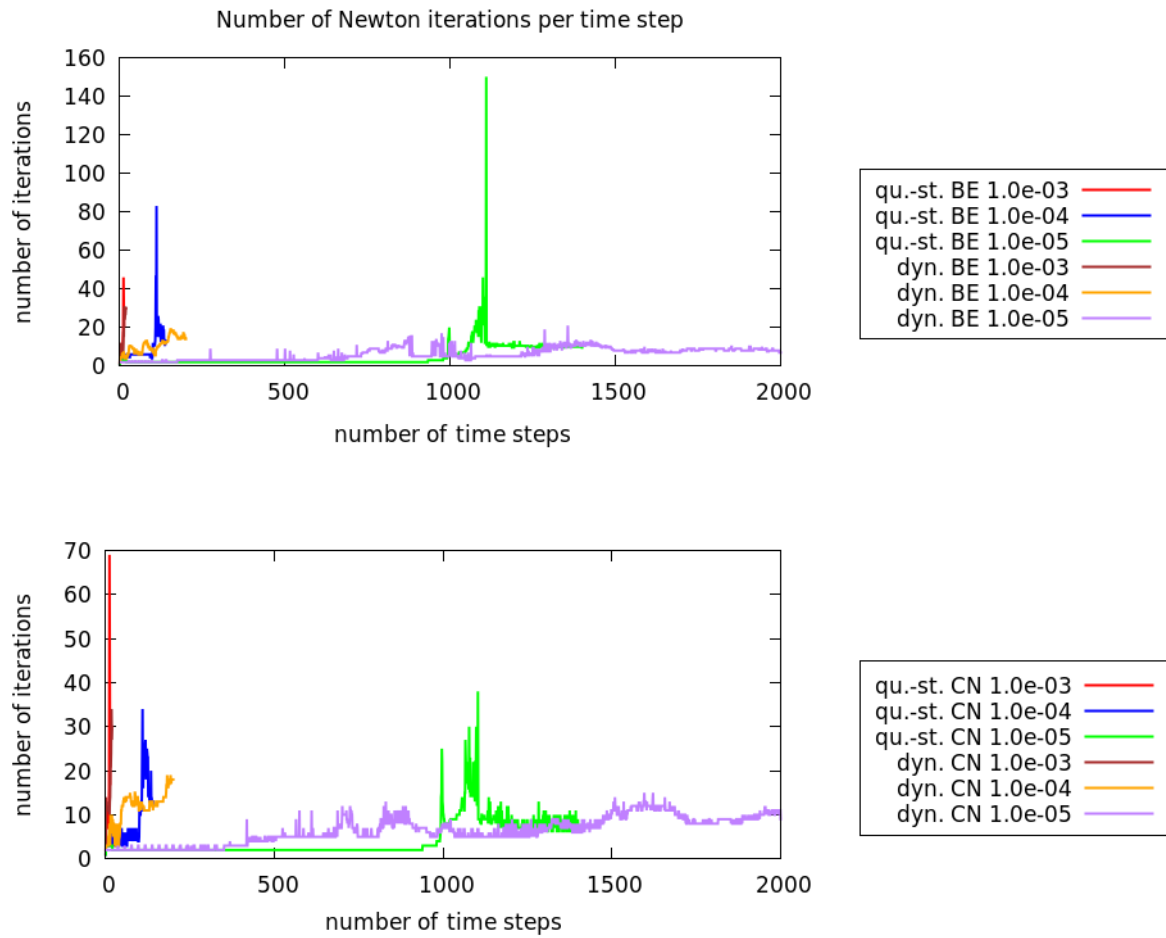
FIG. 5.12: Comparison of number of Newton iterations per step for the quasi-static and dynamic single edge notched shear test based on a backward Euler and a Crank-Nicolson time-stepping scheme with different time step sizes.

5.7   Comparison of backward Euler and Crank-Nicolson timestepping schemes

In this subchapter, we compare two different time-stepping schemes, backward Euler and Crank-Nicolson, in order of a quasi-static and a dynamic fracture model.

Remark 8 *We do not treat the forward Euler time-stepping scheme in our example since very small time step sizes would be needed to get stable numerical results. Therefore in most cases this scheme is not lucrative in praxis.*

Again, as in the previous chapter, we first take a look at the crack patterns. Figure 5.13 exhibit the crack patterns for the quasi-static case in terms of a backward Euler and a Crank-Nicolson scheme. We indicate that the crack reaches the boundary a little bit faster if we apply Crank-Nicolson instead of backward Euler. In the dynamic case, see Figure 5.14, the behavior is obviously, the crack spreads out slower using Crank-Nicolson.

Figure 5.15 shows the comparison of the load-displacement curves in quasi-static fracture for backward Euler and Crank-Nicolson. We inspect the intermediate time step sizes, bisecting time step size δt=1.0e-04s, respectively δt=1.0e-05s, three times. There are no big differences between both time-stepping schemes. The same examination is given in Figure 5.16 using the dynamic fracture model. Here, we can observe completely difference between both time-stepping schemes. The load-displacement curves have an inverse oscillating behavior, comparing backward Euler and Crank-Nicolson in all time step sizes that were used.

Next, we take a look at Figure 5.17 where the number of Newton iterations per time step for the quasi-static model in terms of a backward Euler and a Crank-Nicolson scheme is depicted. Up to the time where the fracture starts growing, both time-stepping schemes have nearly the same behavior. For times where the fracture grows there is a highly increase of Newton steps for certain time step sizes. This peak is independent from the time-stepping scheme. For some time step sizes a backward Euler scheme is cheaper, for other ones a Crank-Nicolson scheme is preferably. In terms of the augmented Lagrangian iterations needed to reach the tolerances and in terms of convergence, both time-stepping schemes are almost identical. Figure 5.18 shows the dynamic case. There no big differences between backward Euler and Crank-Nicolson could be observed.
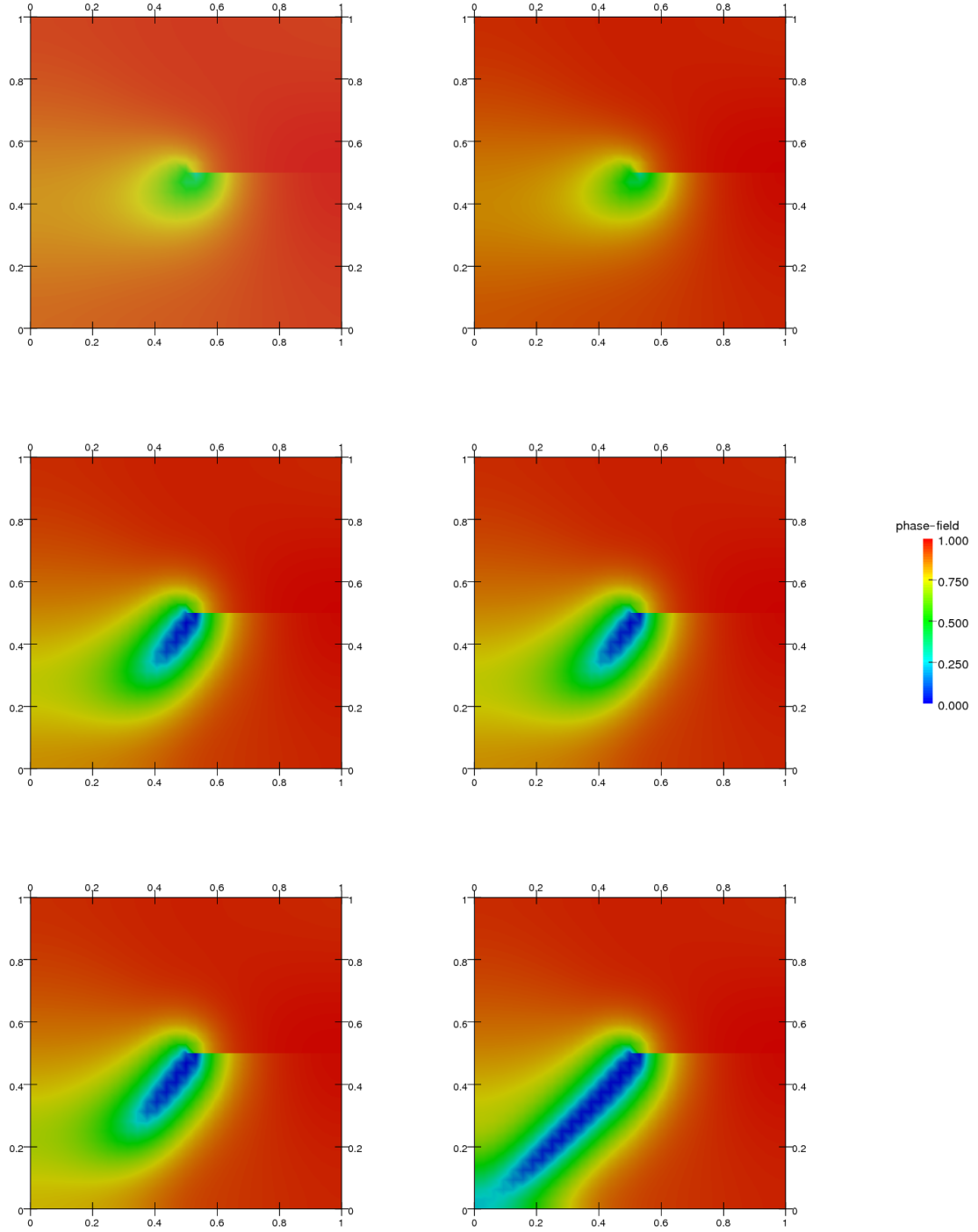
FIG. 5.13: Crack pattern for the quasi-static single edge notched shear test based on a backward Euler scheme (left) and a Crank-Nicolson scheme (right) for time step size ∂t=1.0e-04s. Top: Time T=9.8e-03s, Middle: Time T=1.1e-02s, Bottom: Time T=1.12e-02s.
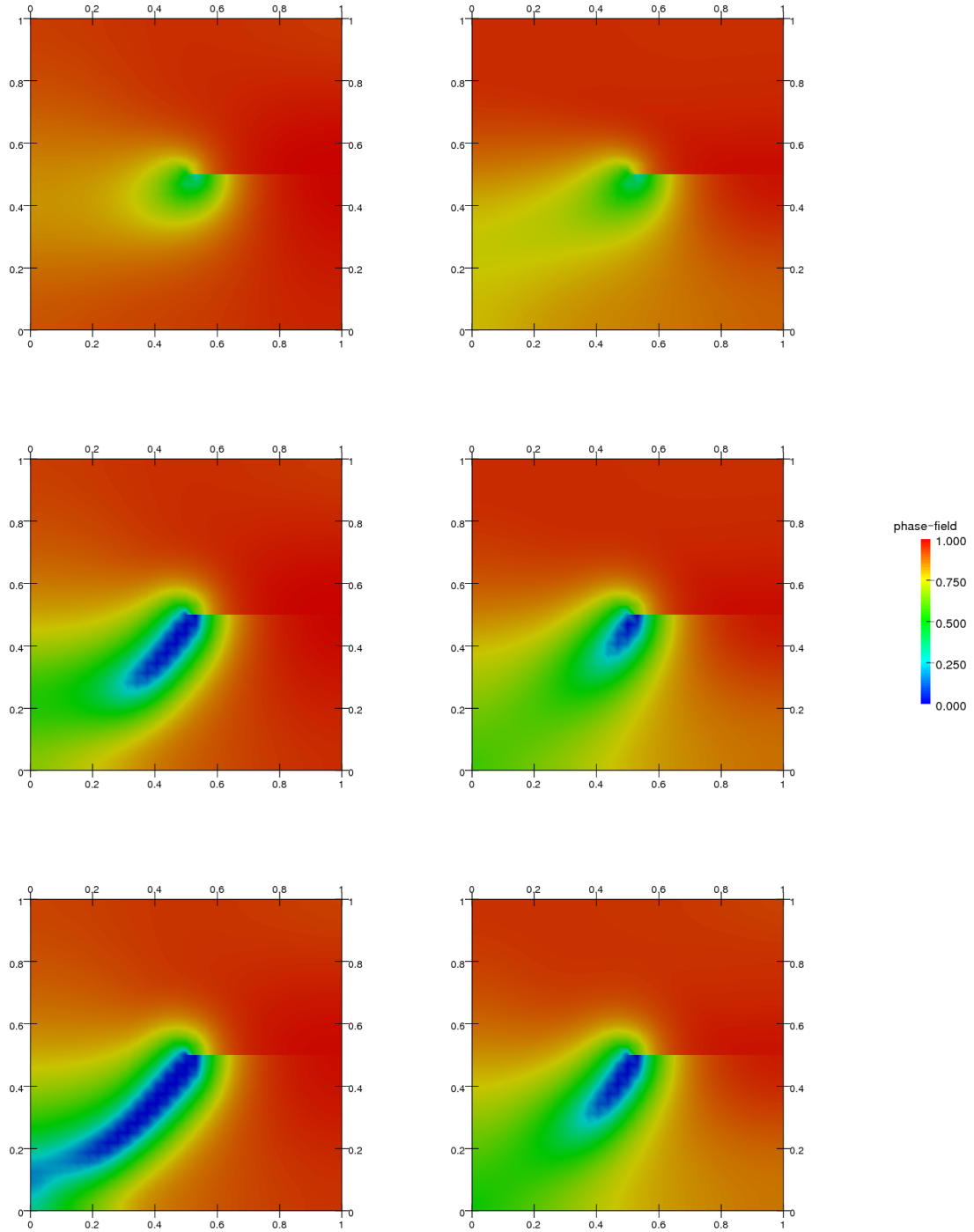
FIG. 5.14: Crack pattern for the dynamic single edge notched shear test based on a backward Euler scheme (left) and a Crank-Nicolson scheme (right) for time step size ∂t=1.0e-04s. Top: Time T=9.8e-03s, Middle: Time T=1.34e-02s, Bottom: Time T=1.44e-02s.
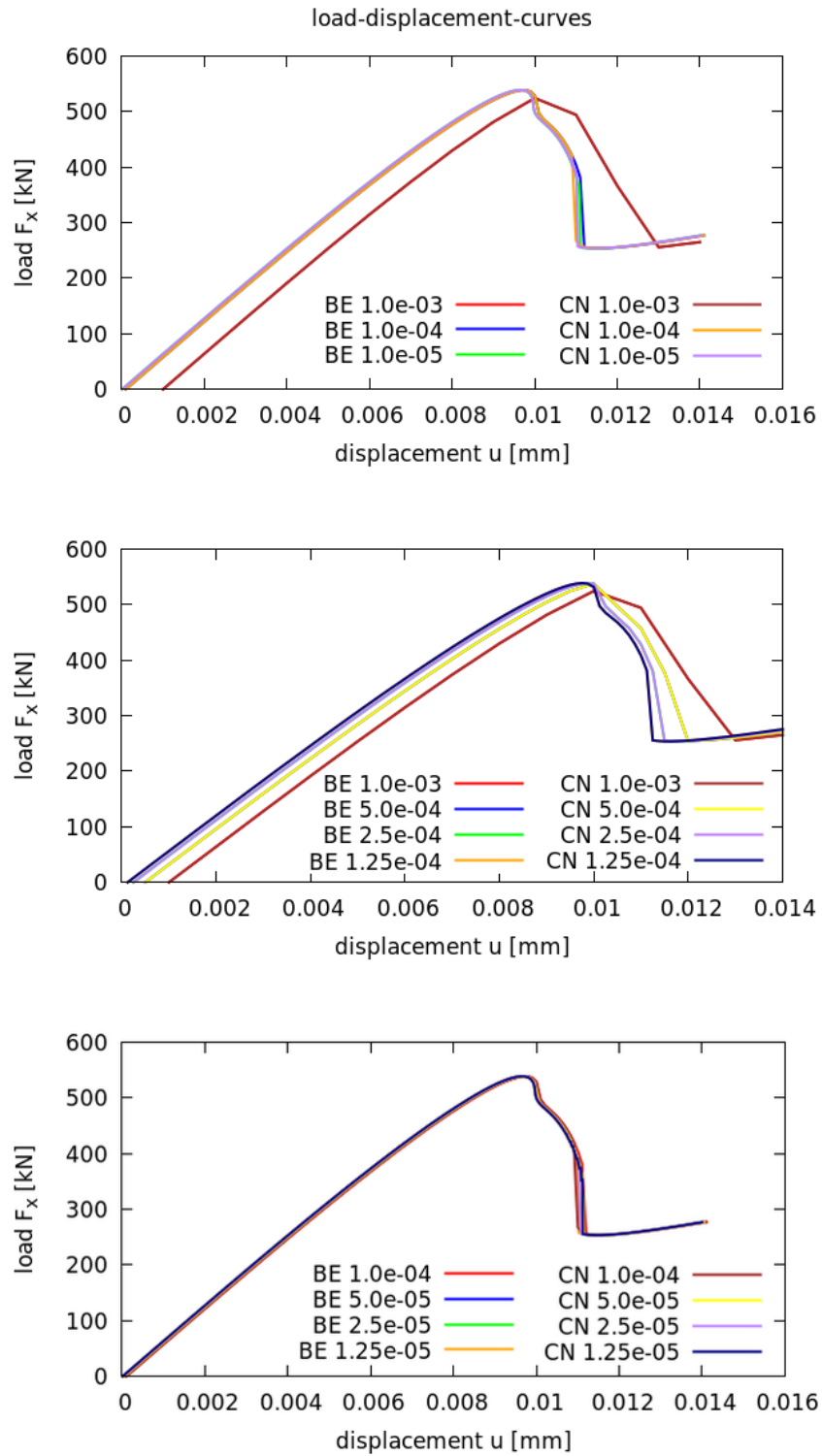
FIG. 5.15: Comparison of the load-displacement curves for the quasi-static single edge notched shear test based on a backward Euler and a Crank-Nicolson time-stepping scheme with different time step sizes.
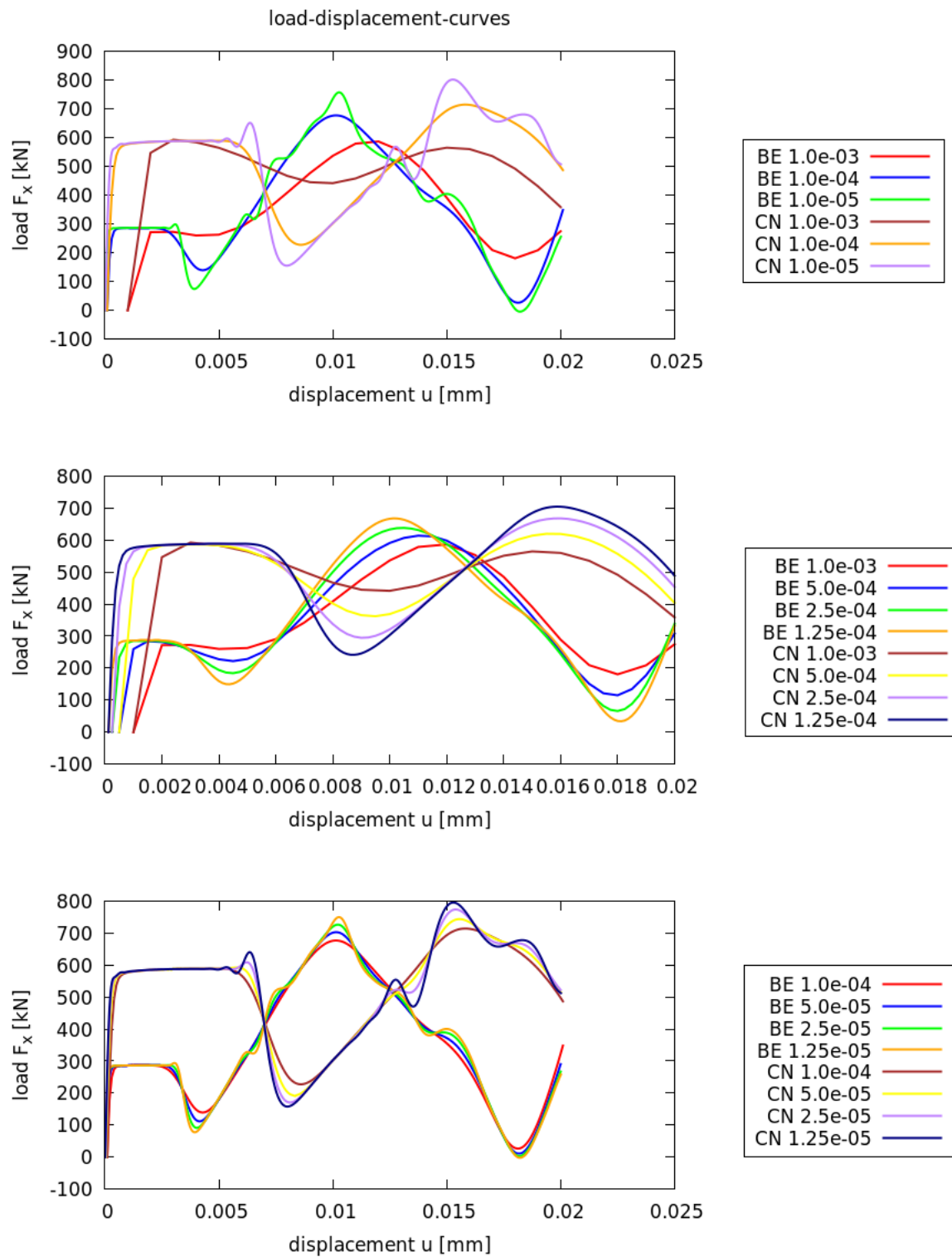
FIG. 5.16: Comparison of the load-displacement curves for the dynamic single edge notched shear test based on a backward Euler and a Crank-Nicolson time-stepping scheme with different time step sizes.
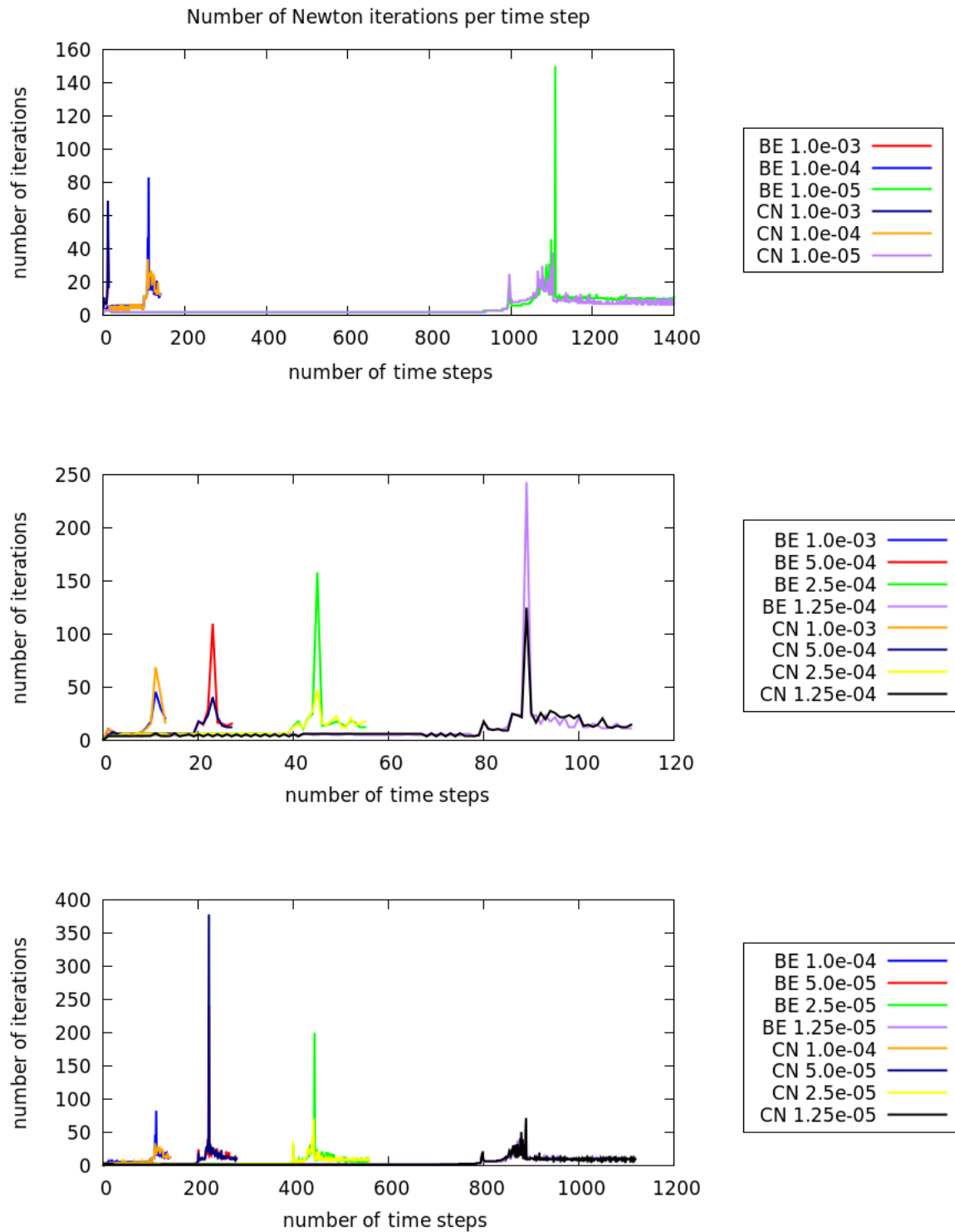
FIG. 5.17: Comparison of number of Newton iterations per step for the quasi-static single edge notched shear test based on a backward Euler and a Crank-Nicolson time-stepping scheme with different time step sizes.
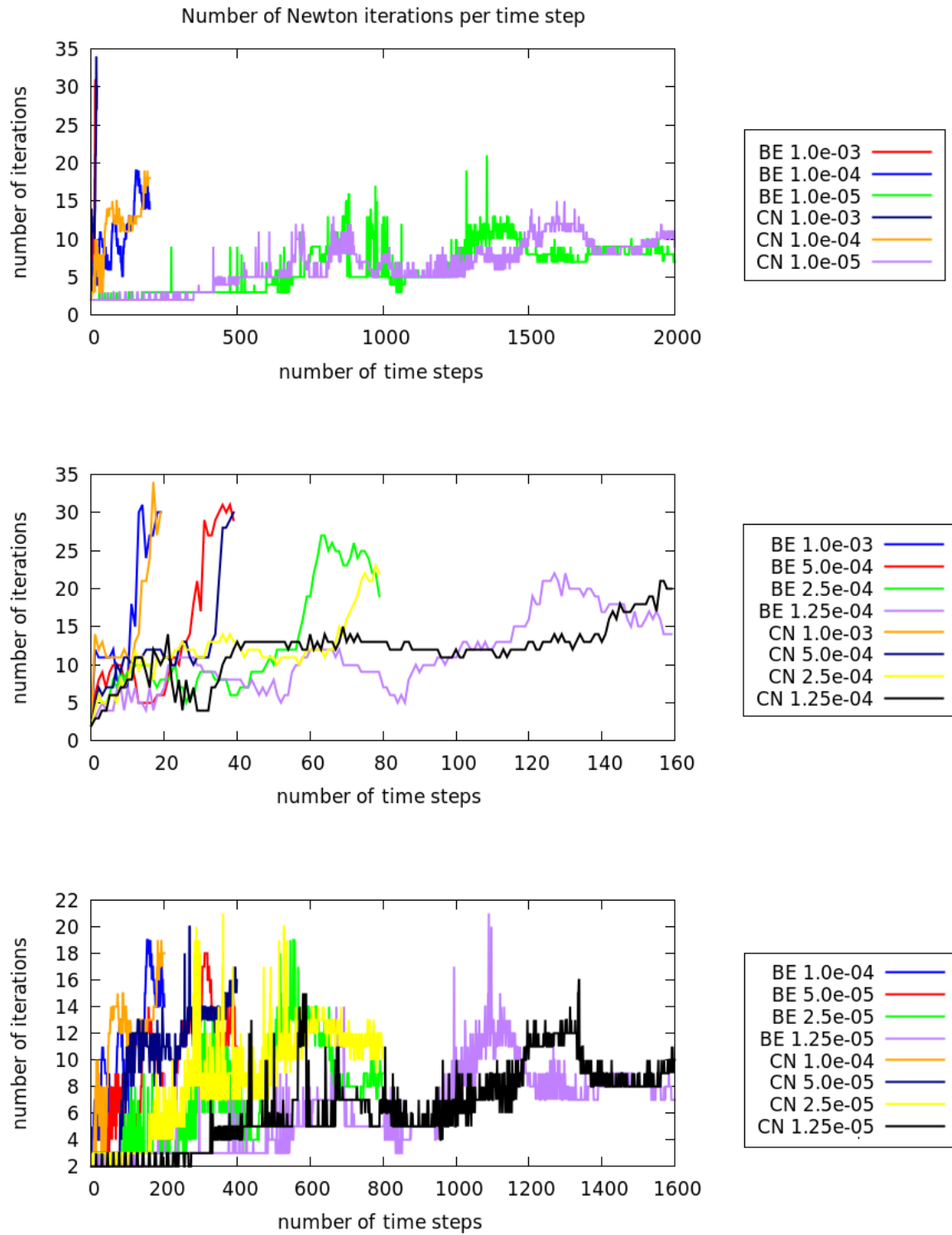
Fɪɢ. 5.18: Comparison of number of Newton iterations per step for the dynamic single edge notched shear test based on a backward Euler and a Crank-Nicolson time-stepping scheme with different time step sizes.

6   Conclusions

In this thesis, we considered a quasi-static phase-field sample including an initial crack, extended it to the dynamic fracture model and showed the differences between them, checking several time-stepping schemes, in case of accuracy and computational costs.

In our example, the single edged notched shear test, a squared specimen involving a horizontal notch was considered. After defining boundary conditions and spectral decomposition of the stress σ into a tensile and a compressive part for a physical reason, we set the parameters to implement this model in the finite element software deal.II. Here, we analyzed with the aid of One-Step-θ schemes different time-stepping schemes, as backward Euler and Crank-Nicolson. We did not treat the forward Euler scheme since there would have been very small time step sizes needed to get stable numerical results.

Considering the crack patterns for different time step sizes, we could observe that the fracture grows slower using the dynamic model. In the dynamic case we could see that a backward Euler scheme is faster then a Crank-Nicolson scheme. For the quasi-static fracture model there is no big difference, using a backward Euler scheme is only a little bit slower in comparison to Crank-Nicolson.

Looking at the load-displacement curves showed, that an effective element size of $h \approx 0.001$mm is needed for both time-stepping schemes. The quasi-static curves are in agreement to [1], there is hardly any difference using Crank-Nicolson instead of backward Euler. The quasi-static fracture model is barely comparable with the dynamic one since the dynamic curves have not the typical behavior of common load-displacement curves. They have an oscillating movement which is even inverse comparing backward Euler and Crank-Nicolson.

Observing the number of Newton iterations, we could see that this number is obviously higher using the quasi-static model. In this model there is a highly increase of Newton steps for certain time step sizes. In the dynamic fracture model the number of Newton iteration rises slowly. The number of Lagrangian iterations is for both fracture models lesser the smaller the time step size is, in general it is a little bit higher in the dynamic case. The smaller the time step size the better the convergence. Also the Jacobian matrix has then to be build less often. This observations hold for both time-stepping schemes, backward Euler and Crank-Nicolson.

Finally we can not obviously say if it is more efficient using the quasi-static or the dynamic fracture model, a backward Euler or a Crank-Nicolson time-stepping scheme. Each of them, models and time-stepping schemes, has both, advantages and drawbacks. This is surprising as one could think Crank-Nicolson should be the better choice in case of its consistency order.

Of course there are lots more open questions on this topic, like the comparison of the monolithic and staggered (i.e., the equations are solved one by one) approach for solving the phase-field equations. This may be a great theme for future studies.

List of Figures

List of Tables

References

[1] WICK T., *An error-oriented newton/inexact augmented lagrangian approach for fully monolithic phase-field fracture propagation*, SIAM J. Sci. Comput., Vol. 39(4) (2017) pp. B589-B617.

[2] WHEELER M., WICK T. AND WOLLNER W., *An augmented-Lagrangian method for the phase-field approach for pressurized fractures*, Comp. Meth. Appl. Mech. Engrg., 271 (2014), pp. 69-85.

[3] MIKELIĆ A., WHEELER F. AND WICK T., *A quasi-static phase-field approach to pressurized fractures*, Nonlinearity, 28 (2015), pp.1371-1399.

[4] MIKELIĆ A., WHEELER F. AND WICK T., *A phase-field approach to the fluid filled fracture surrounded by a poroelastic medium*, SIAM Multiscale Model. Simul., 13 (2015), pp. 367-398.

[5] MIEHE C., HOFACKER M. AND WELSCHINGER F., *A phase field model for rate-independent crack propagation: Robust algorithmic implementation based on operator splits*, Comput. Meth. Appl. Mech. Engrg., 199 (2010), pp. 2765-2778.

[6] BANGERTH W., HARTMANN R. AND KANSCHAT G., *deal.II — a general purpose object oriented finite element library*, ACM Trans. Math. Softw., 33 (2007), pp. 24/1-22/27.

[7] MIEHE C., HOFACKER M. AND WELSCHINGER F., *Thermodynamically consistent phase-field models of fracture: Variational principles and multi-field FE implementations*, Int. J. Numer. Meth. Engng., 83 (2010), pp. 1273–1311.

[8] BORDEN M., VERHOOSEL C., SCOTT M., HUGHES T. AND LANDIS C., *A phase-field description of dynamic brittle fracture*, Comput. Methods Appl. Mech. Engrg., 217–220 (2012), pp. 77-95.

[9] LARSEN C., *Models for dynamic fracture based on Griffith's criterion*, IUTAM Symposium on Variational Concepts with Applications to the Mechanics of Materials, Vol. 21 (2010), pp. 131-140.

[10] LARSEN C., ORTNER C. AND SÜLI E., *Existene of solutions to a regularized model of dynamic fracture*, Mathematical Models and Methods in Applied Sciences, Vol. 20, No. 7 (2010), pp. 1021-1048.

[11] BOURDIN B., LARSEN C. AND RICHARDSON C., *A time-discrete model for dynamic fracture based on crack regularization*, Int J Fract, Vol. 168(2) (2011), pp. 133-143.

[12] HOFACKER M. AND MIEHE C., *Continuum phase field modeling of dynamic fracture: variational principles and staggered FE implementation*, Int J Fract, Vol. 178(1-2) (2012), pp. 113-129.

[13] SCHLÜTER A., WILLENBÜCHER A., KUHN C. AND MÜLLER R., *Phase field approximation of dynamic brittle fracture*, Comput. Mech., Vol. 54(5) (2014), pp. 1141-1161.

[14] BOURDIN B., FRANCFORT A. AND MARIGO J.J., *The variational approach to fracture*, Journal of Elasticity, Vol. 91(1-3) (2008), pp. 5-148.

[15] WICK T., *Coupling fluid-structure interaction with phase-field fracture*, Journal of Computational Physics, Vol. 327 (2016), pp. 67-96.

[16] GROSSMANN C. AND ROOS H.-G., *Numerische Behandlung partieller Differentialgleichungen*, Teubner Studienbücher Mathematik, Auflage 3 (2005).

[17] WICK T., *Modeling, Discretization, Optimization, and Simulation of Fluid-Structure Interaction*, Technische Universität München, Fakultät für Mathematik, Lehrstuhl M17 (2015).

[18] TUREK S., *Efficient solvers for incompressible flow problems*, Lecture Notes in Computational Science and Engineering (1999), pp. 161-168.

[19] TUREK S., RIVKIND L., HRON J. AND GLOWINSKI R., *Numerical analysis of a new time-stepping θ-scheme for incompressible flow simulations*, Ergebnisberichte des Instituts für Angewandte Mathematik Nummer 282, Fakultät für Mathematik, TU Dortmund, 282 (2005).

[20] GRIFFITH A.A., *The phenomena of rupture and flow in solids*, Pshilos. Trans. R. Soc. Lond., 221 (1921), pp. 163-198.

[21] IRWIN G.R., *Elasticity and plasticity: fracture*, Flügge S. (ed.), Encyclopedia of Physics, Vol. 6. Springer (1958), pp. 551-590.

[22] FRANCFORT G.A. AND MARIGO J.J., *Revisiting brittle fracture as an energy minimization problem*, J. Mech. Phys. Solids, 46 (1998), pp. 1319-1342.

[23] BOURDIN B., FRANCFORT G.A. AND MARIGO J.J., *Numerical experiments in revisited brittle fracture*, J. Mech. Phys. Solids, 48 (2000), pp. 797-826.

[24] MUMFORD D. AND SHAH J., *Optimal approximations by piecewise smooth functions and associated variational problems*, Communications on Pure and Applied Mathematics, 42 (1989), pp. 577-685.

[25] AMBROSIO L. AND TORTORELLI V.M., *Approximation of functionals depending on jumps by elliptic functionals via γ-convergence*, Communications on Pure and Applied Mathematics, 43 (1990), pp. 999-1036.

[26] KARMA A., KESSLER D.A. AND LEVINE H., *Phase-field model of mode III dynamic fracture*, Physical Review Letters, 87(4):045501 (2001).

[27] WICK T., *Modified Newton methods for solving fully monolithic phase-field quasi-static brittle fracture propagation*, Comp. Meth. Appl. Mech. Engrg., Vol. 325 (2017), pp. 577-611.

[28] DAVIS T.A. AND DUFF I.S., *An unsymmetric-pattern multifrontal method for sparse LU factorization*, SIAM J. Matrix Anal. Appl., 18 (1997), pp. 140-158.

[29] DEUFLHARD P., *Newton Methods for Nonlinear Problems*, Springer Series in Computational Mathematics, Vol. 35 (2011).

[30] BANGERTH W., GEIGER M. AND RANNACHER R., *Adaptive Galerkin finite element methods for the wave equation*, Comput. Methods Appl. Math., 10 (2010), pp. 3-48.

[31] BRAESS D., *Finite Elemente – Theorie, schnelle Löser und Anwendungen in der Elastizitätstheorie*, Springer-Lehrbuch Masterclass, Auflage 5 (2013).

[32] THOMÉE V., *Galerkin Finite Element Methods for Parabolic Problems*, Springer Series in Computational Mathematics, Second Edition (2006).

[33] CIARLET P.G., *The Finite Element Method for Elliptic Problems*, SIAM Classics in Applied Mathematics, 2nd edition (2002).

[34] GERASIMOV T. AND DE LORENZIS L., *A line search assisted monolithic approach for phase-field computing of brittle fracture*, Comput. Methods Appl. Mech. Engrg., 312 (2016), pp. 276-303.